

THE OPTIMAL VERTICAL ROOT PROFILE UNDER A CHANGING CLIMATE – A MODEL APPROACH –

Master's thesis

in the Master of Science program in Biology

at the University of Hamburg

Year of publication: 2023

Submitted by: Robin Pelchen

Born on: 06.08.1993

Supervisor: Prof. Dr. Philipp Porada

Co-Supervisor: Dr. Christoph Reisdorff

Eidesstattliche Erklärung

Hiermit bestätige ich an Eides statt, dass die vorliegende Arbeit von mir selbständig verfasst wurde und ich keine anderen als die angegebenen Hilfsmittel – insbesondere keine im Quellenverzeichnis nicht benannten Internet–Quellen – benutzt habe und die Arbeit von mir vorher nicht in einem anderen Prüfungsverfahren eingereicht wurde.



Table of Contents

1	Table of Figures	5
2	Table of Tables	7
3	Abstract	8
4	Zusammenfassung	9
5	Introduction	10
6	Material and Methods	14
6.1	Model description	14
6.1.1	Hydraulic pathway	14
6.1.2	Plant physiological processes	15
6.1.3	Carbon balance	16
6.1.4	Strategies	16
6.2	Model parameters	17
6.3	Simulation setup	18
6.3.1	Hypothesis 1: Soil	19
6.3.2	Hypothesis 2: Precipitation	20
6.3.3	Hypothesis 3: Temperature	21
6.4	Evaluation	21
7	Results	22
7.1	Hypothesis 1: Soil	22
7.2	Hypothesis 2: Precipitation	23
7.3	Hypothesis 3: Temperature	27
7.4	Sensitivity analysis	29
8	Discussion	32
8.1	Optimal root profile and soil texture	32
8.2	Optimal root profile and precipitation	35
8.3	Optimal root profile and temperature	37

8.4	Sensitivity analysis	38
8.5	Model limitations.....	39
8.5.1	Hydraulic pathway	39
8.5.2	Plant physiological processes	40
8.5.3	Carbon balance	40
8.6	Model evaluation	41
8.7	Conclusion	41
9	Acknowledgements	43
10	References	44
11	Appendix	51
11.1	Model description	51
11.1.1	Hydraulic pathway	51
11.1.2	Plant physiological processes	55
11.1.3	Carbon balance	59
11.2	Sensitivity analysis.....	59

1 Table of Figures

- Figure 1** Schematic representation of the model framework; Boxes are implemented processes and reservoirs of the hydraulic pathway (blue), plant physiological processes (green) and carbon balance (red). Thin arrows illustrate effects of climate and processes on other processes. Thick arrows illustrate fluxes of water (blue) and carbon (red). 14
- Figure 2** Schematic representation of the implemented strategy; Blue arrows illustrate the hydraulic pathway from the soil through the plant to the atmosphere. Connected with a network of hydraulic conductivities (red). Vertical root distribution is implied by the yellow boxes. 15
- Figure 3** Five different cumulative root fractions Y as a function of z 16
- Figure 4** Soil moisture retention curves of the three soil types: clay, loam, and sand (left) and the hydraulic conductivity as a function of θ (right)..... 20
- Figure 5** Model output of the three soil types; (a) mean annual transpiration (b) drought induced mortality (c) net primary production and (d) efficiency, all displayed vs. the root distribution index β 22
- Figure 6** Model output of the three soil types under the five precipitation scenarios (R_0 , $R_{-20\%}$, $R_{+20\%}$, $RS_{-20\%}$, $RW_{-20\%}$); (a-c) mean annual transpiration (d-f) drought induced mortality (g-i) net primary production and (j-k) efficiency, all displayed vs. the root distribution index β 24
- Figure 7** Model output of the three soil types under the two climate scenarios (P_{79} and P_{00}); (a-c) mean annual transpiration (d-f) drought induced mortality (g-i) net primary production and (j-k) efficiency, all displayed vs. the root distribution index β 28
- Figure 8** Model output of the parameters LAI and BM_{root} of the sensitivity analysis; Low, base, and high values are shown in table 9. 30
- Figure 9** Optimal root profiles of H1; Cumulative root distribution as a function of β . clay: $\beta=0.942$, loam: $\beta=0.971$, sand: $\beta=0.988$ 32
- Figure 10** Optimal root profiles of the precipitation scenarios R_0 , $R_{-20\%}$ and $R_{+20\%}$; Cumulative root distribution as a function of β . Clay: $\beta=0.942$ (R_0), $\beta=0.932$ ($R_{-20\%}$), $\beta=0.944$ ($R_{+20\%}$); Loam: $\beta=0.971$ (R_0), $\beta=0.961$ ($R_{-20\%}$), $\beta=0.978$ ($R_{+20\%}$); Sand: $\beta=0.988$ (R_0), $\beta=0.980$ ($R_{-20\%}$), $\beta=0.990$ ($R_{+20\%}$). 35

- Figure 11** Optimal root profiles of the precipitation scenarios R_0 , $RS_{-20\%}$ and $RW_{-20\%}$; Cumulative root distribution as a function of β . Clay: $\beta=0.942$ (R_0), $\beta=0.942$ ($RS_{-20\%}$), $\beta=0.937$ ($RW_{-20\%}$); Loam: $\beta=0.971$ (R_0), $\beta=0.976$ ($RS_{-20\%}$), $\beta=0.968$ ($RW_{-20\%}$); Sand: $\beta=0.988$ (R_0), $\beta=0.990$ ($RS_{-20\%}$), $\beta=0.985$ ($RW_{-20\%}$). 36
- Figure 12** Optimal root profiles of the climate scenarios P_{79} and P_{00} ; Cumulative root distribution as a function of β . Clay: $\beta=0.922$ (P_{79}), $\beta=0.935$ (P_{00}); Loam: $\beta=0.966$ (P_{79}), $\beta=0.971$ (P_{00}); Sand: $\beta=0.988$ (P_{79}), $\beta=0.988$ (P_{00}). 38
- Figure 13** Model output of the parameter σ of the sensitivity analysis; Low, base, and high values are shown in table 9..... 59
- Figure 14** Model output of the parameters h , z_{\max} and r_r of the sensitivity analysis; Low, base, and high values are shown in table 9..... 60
- Figure 15** Model output of the parameters R_r^* , r_l and K_a of the sensitivity analysis; Low, base, and high values are shown in table 9..... 61
- Figure 16** Model output of the parameters $v_{\max 25}$ and g_{\max} of the sensitivity analysis; Low, base, and high values are shown in table 9..... 62
- Figure 17** Model output of the parameters Ψ_{opt} and Ψ_{50} of the sensitivity analysis; Low, base, and high values are shown in table 9..... 62
- Figure 18** Model output of the parameters M_b and M_Ψ of the sensitivity analysis; Low, base, and high values are shown in table 9..... 63

2 Table of Tables

Table 1 Overview of parameters and natural constants used in the model; Parameters marked with ** are included in a sensitivity analysis.	17
Table 2 Overview of the soil parameters obtained from Carsel and Parrish (1988) describing the three soil types: clay, loam, and sand.	19
Table 3 Precipitation of the five scenarios: R_0 , $R_{-20\%}$, $R_{+20\%}$, $RS_{-20\%}$, $RW_{-20\%}$. Separated according to mean annual precipitation, mean summer precipitation, and mean winter precipitation.	20
Table 4 Mean of the climate input of the two climates before the year 2000 (P_{79}) and after (P_{00}).....	21
Table 5 Minimum and maximum values of the model output of the three soil types: mean annual transpiration, drought induced mortality, net primary production, and efficiency; with the associated root distribution index β	23
Table 6 Minimum and maximum values of the model output of the three soil types under the five precipitation scenarios (R_0 , $R_{-20\%}$, $R_{+20\%}$, $RS_{-20\%}$, $RW_{-20\%}$): mean annual transpiration, drought induced mortality, net primary production, and efficiency; with the associated root distribution index β	25
Table 7 Potential evapotranspiration and the potential evapotranspiration during summer of the two climate scenarios.....	27
Table 8 Minimum and maximum values of the model output of the three soil types under the two climate scenarios (P_{79} and P_{00}): mean annual transpiration, drought induced mortality, net primary production, and efficiency; with the associated root distribution index β	28
Table 9 Parameters that were considered in the sensitivity analysis with the associated β of the ORP with high and low values	29

3 Abstract

In the last decades an increased tree mortality and exceeded canopy defoliation was observed in European forests. These were associated with more intense drought events because of climate change. In those cases, soil water is absorbed by the root system and limited water supply can lead to cavitation. However, trees can reduce the risk of cavitation by adjusting their stomata conductance to adapt their transpiration rate to the root water uptake capacity. Thus, a tradeoff arises between carbon assimilation and the prevention of cavitation. An optimal adapted root system to the hydraulic conditions increases the root water uptake capacity, allowing trees to maintain longer periods with their stomata open. The high variety of different vertical root profiles across biomes, plant function types, and species - determined by environmental factors such as temperature, precipitation, duration of the dry season, and soil texture - suggests that trees should adapt their root systems in response to a changing climate. The aim of this study was to identify the optimal vertical fine root distribution for a North German climate and to show how these change under a changing climate. For that, a process-based model was developed to simulate the hydraulic pathway from the soil through the plant to the atmosphere and link the plant water status with plant physiological processes, such as stomata and photosynthesis. Within the model framework trees were tested with different vertical fine root distributions and their success in terms of carbon assimilation was evaluated. The effect of soil texture, precipitation and temperature on the optimal root profile were tested. The results suggest that optimal root profiles are progressively deeper distributed from fine textured clay soil to medium textured loamy soil to coarse textured sandy soil. Following the faster and deeper infiltration of rainwater due to a higher hydraulic conductivity in more coarser soils. A decrease of mean annual precipitation lead to more shallower root profiles, while an increase of mean annual precipitation resulted in deeper distributed roots. Changes in the seasonality of precipitation while the mean annual precipitation was equal resulted in deeper root profiles with increased winter precipitation and vice versa to shallower root profiles with increased summer precipitation. No effect on the optimal root profile with increasing temperature could be observed, due to minor differences in the climate data and a simplified approach of estimating potential evapotranspiration. However, the general patterns of the results are supported by the literature and seem plausible under the assumption that water is the limiting factor. The here presented study gives insight into how root systems might adapt to climate change, where changes in the precipitation patterns are predicted.

4 Zusammenfassung

Intensivere Trockenperioden aufgrund der Klimaerwärmung führten in den letzten Jahrzehnten zu einem erhöhten Waldsterben in Europa. Bäume nehmen Bodenwasser mit ihrem Wurzelsystem auf, ist dieses limitiert, steigt das Risiko von Kavitation. Mithilfe der Stomata können Bäume ihren Wasserverlust aufgrund von Transpiration verringern, dies führt jedoch zu einer reduzierten Kohlenstoffassimilation. Ein an die Wasserbedingungen optimal angepasstes Wurzelsystem erhöht die Menge an absorbierbarem Wasser und ermöglicht es den Bäumen, ihre Stomata länger geöffnet zu halten. Die große Vielfalt an verschiedenen Wurzelprofilen in verschiedenen Biomen und Arten – bestimmt durch Umweltfaktoren wie Temperatur, Niederschlag, Dauer der Trockenperiode und Bodenbeschaffenheit – legt nahe, dass Bäume ihr Wurzelsystem als Reaktion auf den Klimawandel anpassen sollten. Das Ziel dieser Studie war es, das optimale Wurzelsystem für ein norddeutsches Klima zu identifizieren und die Auswirkungen von Klimaveränderungen auf dieses zu untersuchen. Dafür wurde ein prozessbasiertes Modell entwickelt, das den Wasserkreislauf vom Boden durch die Pflanze zur Atmosphäre simuliert und diesen mit pflanzenphysiologischen Prozessen, wie stomatäre Leitfähigkeit und Photosynthese verbindet. In dem Modell wurden Strategien mit unterschiedlichen vertikalen Feinwurzelverteilungen getestet und ihr Erfolg in Bezug auf ihre Kohlenstoffbilanz bewertet. Die Effekte von Bodentextur, Niederschlag und Temperatur auf das optimale Wurzelprofile wurden untersucht. Die Ergebnisse zeigten, dass optimale Wurzelprofile in fein strukturierten Böden flacher und in grob strukturierten Böden tiefer verteilt sind. Bäume passen dabei ihr Wurzelsystem an die Infiltrationseigenschaften des Bodens an, welche aufgrund einer höheren hydraulischen Leitfähigkeit schneller und deshalb tiefer ist. Eine Reduzierung der jährlichen Niederschlagsmenge führte zu flacheren optimalen Wurzelprofilen, während eine Erhöhung des Niederschlags zu tieferen Wurzeln führte. Eine Veränderung der Niederschlagsmuster bei gleichbleibendem Jahresniederschlag führte bei erhöhtem Winterniederschlag zu tieferen Wurzelprofilen und umgekehrt zu flacheren Wurzeln bei erhöhter Niederschlagsmenge im Sommer. Aufgrund nur kleiner Temperaturunterschiede im vorhandenen Klimadatensatz und einer vereinfachten Methode zur Berechnung der potenziellen Evapotranspiration, konnte kein Effekt der Temperatur auf das optimale Wurzelsystem festgestellt werden. Die allgemeinen Muster der Ergebnisse werden jedoch durch die Literatur unterstützt und sind unter der Annahme, dass Wasser der begrenzende Faktor ist, plausibel.

5 Introduction

There is a high diversity in root systems observed across various biomes, plant function types, and even within the same species (Jackson et al. 1996; Schenk and Jackson 2002; Xu and Li 2008). Thereby, plants adapt their root system to various environmental conditions, adjusting both in the short and long term (Schenk and Jackson 2002; Meier et al. 2018). The main functions of the plant root system are the anchorage in the soil and absorbing nutrients and water (Hodge et al. 2009). While the most limiting nutrients for plant productivity, N, P and K, are higher concentrated in the topsoil (Jobbágy and Jackson 2001), soil moisture profiles occur to be more dynamic and are determined by multiple environmental factors, such as climate and soil properties (Seneviratne et al. 2010; Huang et al. 2016). The development of deep roots provide access to deeper water reservoirs, which can be crucial for the survival of plants, especially during dry periods (Pierret et al. 2016). However, resources in the soil are potentially unevenly distributed and require a tradeoff between a shallower or deeper distributed root profile to balance water and nutrient uptake (Ho et al. 2005). Usually, shallow root profiles have several advantages over a deeper one beyond nutrients accessibility (Schenk 2008). Those include lower energy costs for construction, maintenance and resource uptake, high water availability close to the surface, which is wetted even after small precipitation events and decreasing the probability of oxygen deficiency (Schenk 2008). Consequently, root profiles are generally as shallow as possible and only as deep as necessary to maintain transpiration demand (Schenk 2008).

On a global average, trees have 60% of their roots allocated in the upmost 30 cm of the soil, while biome specific differences can be observed, such as shallower root profiles in boreal forests compared to tropical forests and the even deeper distributed root profiles in temperate deciduous and coniferous forests (Jackson et al. 1996). Most of these patterns can be explained by climate and soil properties (Schenk and Jackson 2002). In water-limited ecosystems, roots tend to be deeper distributed and are positively correlated with annual potential evapotranspiration (PET), annual precipitation and the duration of the warm season. Furthermore, deeper roots are mainly found in coarse-textured sandy soils compared to fine-textured loamy and clay soils (Schenk and Jackson 2002). The work of Fan et al. (2017) specify these findings, by showing a strong sensitivity of rooting depth to the soil moisture profile, determined by infiltration depth and the depth of the water table and its capillary rise. In coarser soils, water infiltrates faster due to their higher hydraulic conductivity. Consequently, it is more challenging for root systems to absorb water before it is lost through drainage. To optimize water uptake, root profiles are deeper distributed in coarser soils (Collins and Bras 2007).

However, the infiltration and soil moisture profiles are also determined by annual precipitation, precipitation patterns and water loss through evaporation in the upper soil layer (Rose 1996; Seneviratne et al. 2010). Drought periods, with no or only small precipitation events and high temperatures resulting in higher PET, are challenging for plants, and are associated with forest defoliation and increased tree mortality in Europe (e.g., Češljar et al., 2022; Obladen et al., 2021; Senf et al., 2020). As a consequence of climate change, increasing temperatures, changes in precipitation patterns, and severe drought periods are more likely to occur (Teuling 2018; IPCC 2022) and make soil moisture a limiting factor for plants in Europe (Grillakis 2019).

Drought induced tree mortality is complex, and not yet fully understood (Hartmann et al. 2018). The hydraulic framework, proposed by McDowell et al. (2008) incorporates two underlying physiological mechanism - carbon starvation and hydraulic failure, both amplify the vulnerability to biotic agents such as insects and pathogens. Hydraulic failure occurs when the root system's water uptake cannot supply the demands of transpiration (McDowell et al. 2008; Hartmann 2010). Water absorbed by the root system moves through the xylem vessel system and diffuses through the stomata, driven by a negative water potential gradient towards the atmosphere (Hartmann et al. 2018). However, in this case of hydraulic failure, the negative pressure within the xylem increases until it causes cavitation and subsequent rupture of the water column, resulting in a partial loss of xylem conductivity (Tyree and Zimmermann 2002), leading to a reduction in photosynthetic productivity and tissue damage (Tyree 2003; Li et al. 2015). Vulnerability to cavitation, often quantified by a Ψ_{50} -value (xylem pressure at which 50% loss of conductivity occurs), varies among species and depends on multiple xylem vessel traits, such as vessel diameter, vessel wall resistivity and pit structure (Tyree et al. 1994; Jacobsen et al. 2005; Scholz et al. 2013; Oeda et al. 2017). Establishing a more stable xylem system is a time-demanding process. However, in short-term, trees can adjust their stomata aperture to reduce the demand of transpiration (Hartmann 2010). Yet, even with stomata conductance reduced to a minimum, trees still lose water by diffusion through the cuticle and the potential of cavitation remains (Ristic and Jenks 2002; Anderegg et al. 2012).

Additionally, the reduction of stomata conductance not only reduces the transpiration rate, but also limits the diffusion of atmospheric CO₂ into the leaves, resulting in a reduced rate of carbon assimilation (Farquhar and Sharkey 1982). Trees consistently require carbohydrates, which are produced during photosynthesis using intracellular CO₂, such as for respiration, root exudates, volatile emissions and production of new leaves, fine roots, and woody compartments (Chapin and Eviner 2007; Hartmann et al. 2020). Limitations in carbon assimilation over an extended period can cause carbon starvation if the demand for carbon cannot be met (McDowell et al.

2008; Hartmann 2010). In the literature, the sum of assimilation and the loss through respiration define the net primary production (NPP) and describe the amount of energy that enters the ecosystem (Chapin and Eviner 2007). In this study, NPP was defined for the tree level and also includes mortality and turnover rates of leaves and fine roots, as these carbon sinks are not available for growth and reproduction. NPP therefore offers an approach to evaluate the success of trees. Under the assumption that water is the limiting factor, trees should adapt their root system to the environmental conditions to maximize their NPP and avoid cavitation.

The investigations of root systems in the field can be challenging. However, a better understanding of the processes defining an optimal root system could contribute to a better understanding of changes in species composition and carbon balances of forests in the future. Several methods for investigating root systems are described in the literature (Alani and Lantini 2020). These methods are either destructive, unsuitable for *in vivo* investigations, or non-destructive but come with certain limitations. For instance, minirhizotrons, commonly used for investigating root dynamics, are restricted by only providing a small viewing window and therefore not capable of identifying the whole root profile (Majdi 1996; Alani and Lantini 2020). Ground penetrating radar represents another non-destructive method capable of identifying the vertical distribution of roots (Alani and Lantini 2020). However, its resolution does not allow the identification of water absorbing fine roots and give no information about other with drought resistance related root traits, such as specific root length (Eissenstat et al. 2000; Ostonen et al. 2007).

To overcome the restrictions of investigating roots in the field, a process-based model was developed. However, a model has other limitations and is based on assumptions. Nevertheless, it gives the opportunity to describe biogeochemical processes and test the effects of environmental changes in a controlled setting. The model developed for this study is designed to maximize carbon uptake while avoiding cavitation. This is achieved by coupling the stomata aperture with the plant water status while the plant water status is mainly determined by the ability of trees to absorb soil water and the water loss through transpiration. When trees are unable to absorb enough soil water to maintain the demand for transpiration, Ψ_{leaf} (Leaf water potential) drops below a threshold leading to an increasing drought induced mortality (M_{Ψ}) to simulate cavitation damage. By reducing the stomata conductance, the demand for transpiration can be reduced with the consequence of a reduced carbon assimilation rate. In the model, stomata are limited by light and additionally only by factors related to the plant water status, namely soil moisture content (θ), Ψ_{leaf} and vapor pressure deficit (VPD). The restrictions of this approach will be discussed. However, strategies were identical in their stomatal behavior

and in all other aspects, except of the vertical fine root distribution, described with the root distribution index β . This made it possible to compare the strategy efficiency only influenced by the root profile and therefore different conditions for absorbing soil water. The processes and the assumptions of the model are described in the section ‘Model description’. The limitations of the model and the made assumptions will be discussed.

The aim of this study was to identify the optimal root profile (ORP), which contributes to the highest NPP and therefore the highest BM_{total} at the end of the simulation, while also describing the environmental factors determining the ORP. In the model, the performance of 30 different root profiles from shallow to deep distributed were tested in three different soil types from coarse to fine textured to answer the following hypotheses:

- H1. Soil water profiles, determined by soil properties, impact the vertical fine root distribution of optimal root profiles
- H2. Changes in precipitation patterns affect the vertical fine root distribution of optimal root profiles
- H3. Rising temperatures lead to an increased PET and higher soil evaporation in the upmost soil layer, resulting in a deeper fine root distribution of optimal root profiles

The simulations were performed with the Hamburg ERA5 climate data set including the years 1979 to 2018. For H1, the original data set was used. For H2, the rain data was manipulated to simulate changes in the precipitation patterns. For H3, root profiles were tested under the climatic conditions from 1979 to 1999 and compared with root profiles tested from 2000 to 2019. Further details are available in the section ‘Simulation setup’.

6 Material and Methods

6.1 Model description

The model for this study was developed in a pre-study by Pelchen (not in press). The used equations are described in the section 11.1 in the appendix. The model is structured in three main components: the hydraulic pathway in the soil-plant-atmosphere continuum, plant physiological processes and carbon balance (Figure 1). The components contain interacting processes to identify the ORP within a certain soil type and under the given climatic conditions.

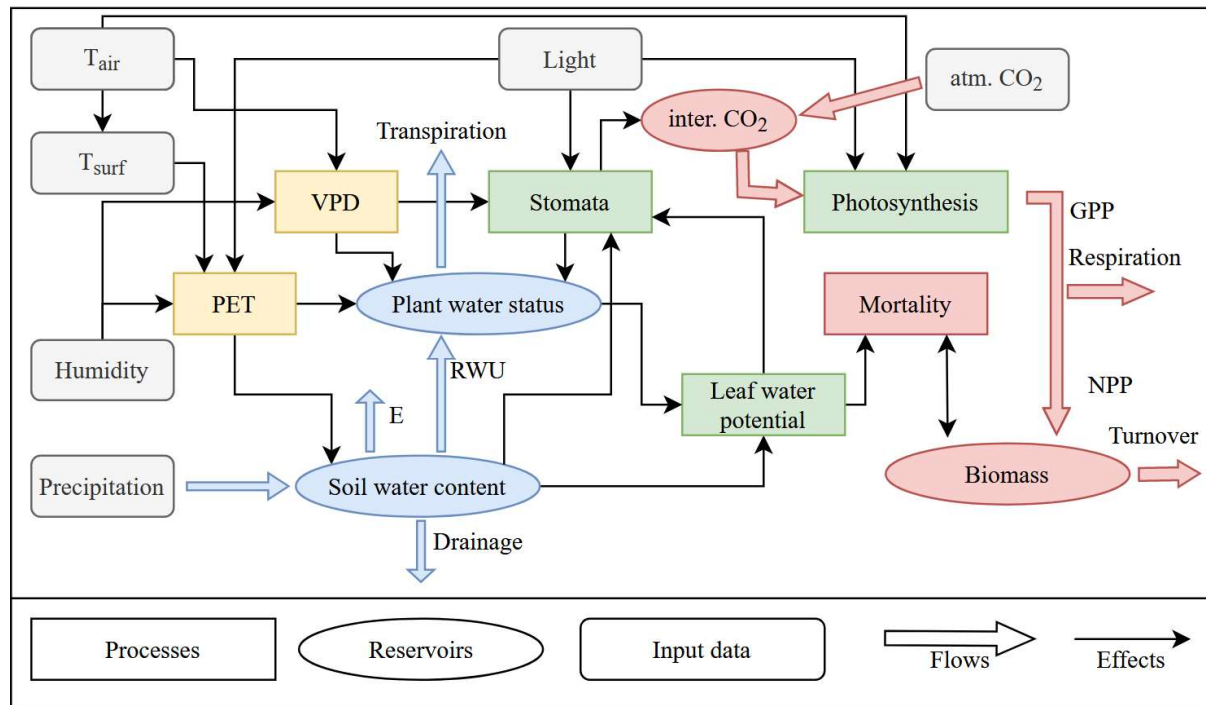


Figure 1 Schematic representation of the model framework; Boxes are implemented processes and reservoirs of the hydraulic pathway (blue), plant physiological processes (green) and carbon balance (red). Thin arrows illustrate effects of climate and processes on other processes. Thick arrows illustrate fluxes of water (blue) and carbon (red).

6.1.1 Hydraulic pathway

The hydraulic pathway includes the infiltration of precipitation in the first soil layer and redistribution of water between adjusted layers, calculated with a general derivation of the finite difference approximation of the Richards Equation (Richards 1931; Bonan 2019c). The soil had a depth of 5 m separated into soil layers each 0.1 m thick. In the soil the fine root biomass (BM_{root}) was distributed, following an asymptotic equation (Eq. 1) first introduced by Gale and Grigal (1987). Depending on the vertical fine root distribution in the soil column, trees were able to absorb soil water and transpire it through the stomata. The water pathway from the soil to the plant to the atmosphere is described with a network of parallel and in series connected hydraulic conductance's (Figure 2) and were combined to the total plant conductance (K_{plant}),

following Ohm's Law (Bonan 2019b). In the model, a steady-state transpiration was considered so that root water uptake equals transpiration. While the main driver for transpiration is the potential evapotranspiration (PET) described with a simplified form of the Penman-Monteith equation, focusing mainly on radiation (Priestley and Taylor 1972). PET was then fractioned into soil evaporation (E) and leaf transpiration (T) (Ritchie 1972).

6.1.2 Plant physiological processes

The plant water status is described with the leaf water potential (Ψ_{leaf}), calculated by applying Darcy's Law with the steady-state transpiration (Bonan 2019b). It was assumed that Ψ was equal in all plant tissues, including xylem and roots. When RWU is not capable to meet the demand of transpiration Ψ_{leaf} drops below a threshold and the risk of cavitation increases. In the model the risk of cavitation is described by a vulnerability curve, describing the percentage loss of conductivity (Pammenter and Willigen 1998). In the model, $\Psi_{\text{leaf,min}}$, the threshold before cavitation becomes critical was defined at 12% loss of conductivity. By reducing the stomata conductance, the

demand of transpiration can be reduced to minimize the risk of cavitation. In the model stomata are limited by soil water content (θ), light, vapor pressure deficit (VPD) and Ψ_{leaf} , following an adapted approach of Jarvis (1976). Stomata conductance not only reduces the transpiration rate it also limits the diffusion of atmospheric CO₂ into the leaves. And therefore, limits the photosynthetic rate, described with the photosynthesis model for C3 species from Farquhar, von Caemmerer and Berry (FvCB model) (Farquhar et al. 1980).

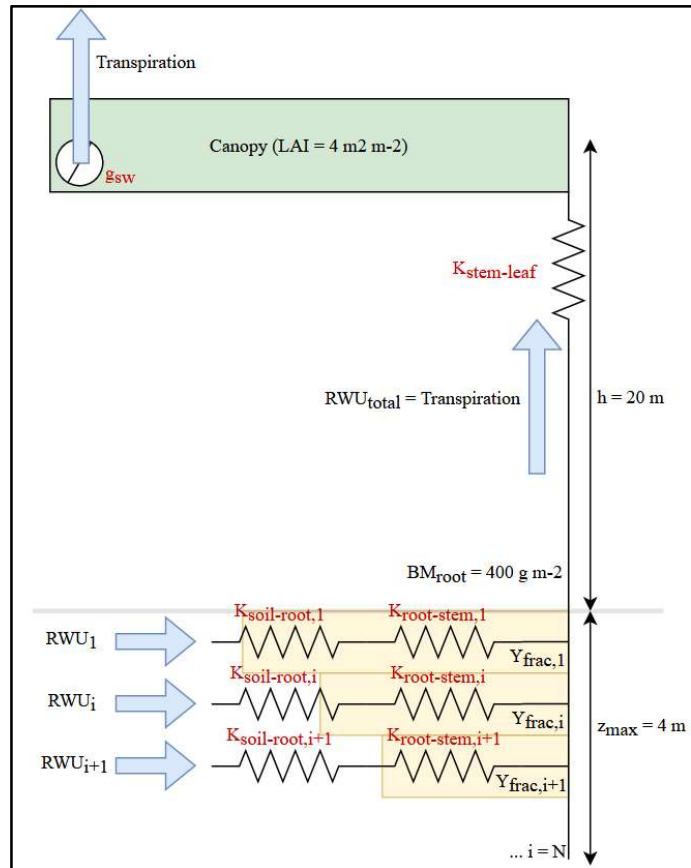


Figure 2 Schematic representation of the implemented strategy; Blue arrows illustrate the hydraulic pathway from the soil through the plant to the atmosphere. Connected with a network of hydraulic conductivities (red). Vertical root distribution is implied by the yellow boxes.

6.1.3 Carbon balance

A simplified biomass accumulation approach was implemented to evaluate the impact of different root profiles on the biomass accumulation. Assimilated carbon is the gross primary production (GPP). The sum of leaf respiration, yearly turnover of leaf and fine root biomass, background mortality (M_b) and drought induced mortality (M_ψ) is defined as the total carbon loss (M_{total}). The sum of GPP and M_{total} is the net primary production (NPP) of the individual tree and defines the tree success. The root profile with the highest NPP leads to the highest BM_{total} at the end of the simulation and was defined as the ORP.

6.1.4 Strategies

The model was developed to simulate individual tree strategies in one dimension (m^2). The simulated trees, subsequently named strategies, were equal in all aspects, except for the vertical fine root distribution. All strategies had a fixed tree height (h) of 20 m, one canopy layer with a leaf area index (LAI) of $4 m^2 m^{-2}$ and a total fine root biomass (BM_{root}) of $400 mg m^{-2}$, which is approximately the fine root biomass of *Fagus sylvatica* (Finér et al. 2007). The biomass accumulation in the model is semi-dynamic. Although, the mortality rates depend on the actual total Biomass (BM_{total}) accumulated over time, there is no direct feedback to the characteristics (LAI, BM_{root} , h) of the strategies included. The consequence of this approach is that strategies can theoretically have a negative BM_{total} and still have an LAI of $4 m^2 m^{-2}$ and a BM_{root} of $400 g m^{-2}$ with consistent root distribution. However, this allows the comparison of root profile performance across the entire simulation period, unaffected by potential negative feedback from ‘bad’ years. Further, strategies were simulated separately; no competition was included.

The vertical distribution of fine root biomass in the soil was described by an asymptotic equation, developed by Gale and Grigal (1987):

$$Y = 1 - \beta_{root}^z \quad (1)$$

where Y is the cumulative root fraction from the soil surface to a certain depth z with β as the describing factor for vertical root distribution. Low values of β describe a shallower root profile (e.g., 0.92) and high values of β are associated with deeper distributed root profiles (e.g., 0.97) (Figure 3). Cumulative root fraction was then converted to root fraction per soil layer (Y_{frac})

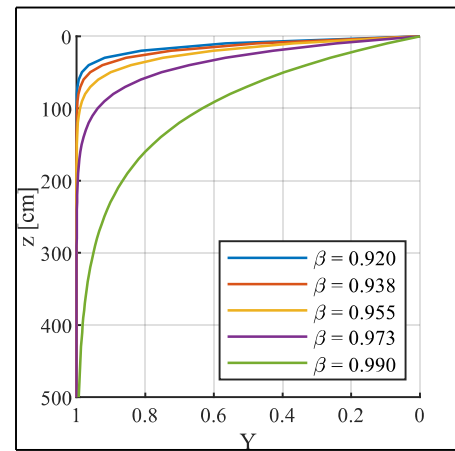


Figure 3 Five different cumulative root fractions Y as a function of z .

and multiplied by total fine root biomass to obtain the fine root biomass per soil layer. To avoid access to the water table, rooting depth was limited by z_{\max} , Y below the water table was then evenly distributed to the upper soil layers, so that $\sum Y_{\text{frac}}=1$. It was assumed that fine roots are evenly distributed within a soil layer.

The model was coded in MATLAB R2023b, and the code can be contained by contacting the author (robin.pelchen@uni-hamburg.de).

6.2 Model parameters

Most of the processes described above are parameterized and most of the parameters were taken directly from the associated literature. The rest of the parameters are estimated either by common knowledge or estimated by educated guess.

Due to our steady-state strategy approach, all parameters are consistent throughout a single simulation run, except for the root distribution index (β). However, some of the used parameters were assumed to be more influential to the ORP than others. For these parameters, a sensitivity analysis with values above and below of the used value has been executed. The ORP's were then compared to each other to determine the effects of these parameters on the model output. Sensitivity analyses were performed in loamy soil over a 20-year period with 15 different rooting strategies, linear distributed from $\beta=0.92$ to $\beta=0.99$. All parameters used in the model are listed in Table 1 and highlighted in case a sensitivity analysis has been executed.

Table 1 Overview of parameters and natural constants used in the model; Parameters marked with ** are included in a sensitivity analysis.

Description	Symbol	Value	Sens. Anal.	Sens. Anal. Low value	Sens. Anal. High value	Unit
General parameters						
Timestep	dt	3600				s
Layer thickness	dz	0.1				m
Soil depth	z	5				m
Water table depth	WT_{depth}	4.9				m
Air pressure	P_{air}	101.8				kPa
Atmospheric CO ₂	CO_2	420				$\mu\text{mol mol}^{-1}$
Atmospheric O ₂	O_2	210				mmol mol^{-1}
Density of water	ρ_w	1000				kg m^{-3}
Molar mass of carbon	m_{Carbon}	12.01				g mol^{-1}
Gravitational acceleration	g	9.81				m s^{-2}
Universal gas constant	R	8.314				$\text{J K}^{-1} \text{mol}^{-1}$
Fraction parameter for PET	σ	0.4	**	0.3	0.5	
Ground heat flux	G	0.0				W m^{-2}
Priestley-Taylor parameter	α	1.3				
Emissivity of the soil surface	ϵ_R	0.97				
Albedo of the soil surface	α_R	0.15				
Psychrometric constant	γ	65.0				$\text{kg m s}^{-2} \text{m}^{-2} \text{K}$
Boltzmann constant	σ_R	5.67e-8				$\text{W m}^{-2} \text{K}^{-4}$
Latent heat evaporation of water	λ	2.45e6				J kg^{-1}
Plant parameters						
Tree height	h	20	**	10	30	m
Maximum rooting depth	z_{\max}	4				m
Leaf area index	LAI	4	**	2	6	$\text{m}^2 \text{m}^{-2}$
Total Biomass at $t=0$	$BM_{\text{total}}(t=0)$	10				kg
Fine root biomass	BM_{root}	400	**	200	600	g

Specific leaf biomass	BM_{leaf}	100				g LAI ⁻¹
Mean fine root radius	r_r	0.29	**	0.01	0.6	mm
Root resistivity	R_r^*	25	**	20	30	MPa s g mmol ⁻¹
Root tissue density	ρ_r	310				kg m ⁻³
Specific root length	r_l	12.2	**	5	20	m g ⁻¹
Stem-to-leaf specific hydr. conductivity	K_a	4	**	2	6	mmol LAI ⁻¹ s ⁻¹ MPa ⁻¹
Photosynthesis						
Reference respiration	R_{d0}	0.9				μmol m ⁻² s ⁻¹
Reference temperature for respiration	T_0	20				°C
Michael-Menten constant for Carbon	K_{C25}	404				μmol mol ⁻¹
Michael-Menten constant for Oxygen	K_{O25}	278.4				mmol mol ⁻¹
Carbon compensation point	Γ_{25}	42.75				μmol mol ⁻¹
Max. Carboxylation rate	v_{cmax25}	60	**	40	80	μmol mol ⁻¹
Max. electron transport rate	J_{max25}	1.67* v_{cmax25}				μmol mol ⁻¹
Energy of activation for K_{C25}	$\Delta H_{a,KC}$	29365				J mol ⁻¹
Energy of activation for K_{O25}	$\Delta H_{a,KO}$	25948				J mol ⁻¹
Energy of activation for Γ_{25}	$\Delta H_{a,\Gamma}$	23400				J mol ⁻¹
Energy of activation for v_{cmax25}	$\Delta H_{a,vcmax}$	58520				J mol ⁻¹
Energy of activation for J_{max25}	$\Delta H_{a,Jmax}$	37000				J mol ⁻¹
Energy of deactivation for v_{cmax25}	$\Delta H_{d,vcmax}$	129350				J mol ⁻¹
Energy of deactivation for J_{max25}	$\Delta H_{d,Jmax}$	152040				J mol ⁻¹
Entropy term v_{cmax25}	ΔS_{vcmax}	485				J mol ⁻¹ K ⁻¹
Entropy term J_{max25}	ΔS_{Jmax}	495				J mol ⁻¹ K ⁻¹
Stomata						
Max. stomata conductance	g_{sw}	0.4	**	0.3	0.5	mol m ⁻² s ⁻¹
Min. stomata conductance	g_0	0.003				mol m ⁻² s ⁻¹
Slope parameter for light limitation	g_1	0.02				
Slope parameter for VPD limitation	g_2	0.12				kPa ⁻¹
Slope parameter for Ψ limitation	g_3	-2				
Water potentials						
Water potential at which $\beta_{wet}=1$	Ψ_{opt}	-0.05				MPa
50% loss of conductivity	Ψ_{50}	-3.5				MPa
12% loss of conductivity	$\Psi_{leaf,min}$	-2.1				MPa
Slope parameter for the vulnerability curve	α	35.71				
Carbon balance						
Turnover rate for leaves	TO_{leaf}	1				g g ⁻¹ yr ⁻¹
Turnover rate for fine roots	TO_{root}	1				g g ⁻¹ yr ⁻¹
Background mortality	M_b	0.01	**	0	0.1	g g ⁻¹ yr ⁻¹
Drought induced mortality	M_{Ψ}	0.5	**	0.3	0.7	g g ⁻¹ yr ⁻¹

6.3 Simulation setup

Final simulation runs were performed over a 40-year period with a north German climate from 1979 to 2019. Input data were obtained from the ERA5 data set with a spatial resolution of 0.281°x0.281° according to N320 Gaussian grid, and a temporal resolution of 1 hour (Hersbach et al. 2020). Input data includes precipitation, air temperature at 2 m height, shortwave radiation, downwelling longwave radiation, relative air humidity and wind speed in 10 m height. The model is developed one-dimensional with an area of 1 m². In the model growing season spanned over 257th days, starting on the 69th day of each simulated year (Norddeutscher Klimamonitor 2023). To mimic leaf shedding, stomatal conductance was set to zero during the non-growing season. Subsequently, growing season is referred to as summer and non-growing season is referred to as winter. In total, 24 simulation runs were performed. In each simulation

all root strategies were tested with a Ψ_{50} value of -3.5 MPa and a $\Psi_{\text{leaf,min}}$ of -2.1 MPa. $\Psi_{\text{leaf,min}}$ was defined as Ψ_{12} , where 12% loss of conductivity occurs.

To identify the optimal root profile and the underlying processes that determine it, strategies were compared in four categories: annual mean of T, M_{Ψ} and NPP and Efficiency (Eff). Eff is defined as the ratio between the most successful strategy in terms of biomass accumulated at the end of the simulation compared to the other strategies in the given setup. The strategy with Eff=1 was defined as the ORP.

$$Eff(\beta_{\text{root}}) = \frac{BM_{\text{total,end}}(\beta_{\text{root}})}{\max(BM_{\text{total,end}}(\beta_{\text{root}}))} \quad (2)$$

Model output of 30 different root profiles, with β from 0.92 to 0.99, was compared to determine the ORP under the conditions described below. The depth at which 50% of BM_{root} is allocated was calculated using Eq. 1 and used to compare the model output with the literature.

6.3.1 Hypothesis 1: Soil

It was assumed that root profiles tend to be deeper in coarser soils compared to root profiles in finer soils, due to a higher hydraulic conductivity, which allows deeper infiltration (Fan et al. 2017). Water movement in the soil relies on the relationship between soil water content with hydraulic conductivity and matric potential. The latter is known as the soil moisture retention curve. In the model, the soil describing parameters, such as the pore-distribution index n_{vG} , the inverse of the air entry potential α_{vG} , and the hydraulic conductivity at saturation K_{sat} , were obtained from the work of (Carsel and Parrish 1988). These parameters were assumed to be constant for all soil layers. θ_{sat} was assumed to be equal for all soil types in all soil layers with $\theta_{\text{sat}}=0.45$. θ_{res} was approximated as 16% to 24% of θ_{sat} , in respect to the ratios described in Carsel et al. (1988)

Table 2 Overview of the soil parameters obtained from Carsel and Parrish (1988) describing the three soil types: clay, loam, and sand.

	Sandy clay loam	Loam	Sandy loam	Unit
α_{vG}	0.059	0.036	0.075	cm^{-1}
n_{vG}	1.48	1.56	1.89	
K_{sat}	1.31	1.04	4.42	cm h^{-1}
θ_{sat}	0.45	0.45	0.45	
θ_{res}	$0.24 \cdot \theta_{\text{sat}}$	$0.18 \cdot \theta_{\text{sat}}$	$0.16 \cdot \theta_{\text{sat}}$	

To test H1, root strategies were simulated in three different soil types: Sandy loam, loam, and sandy clay loam (Table 2). The soils were classified with their sand and clay content, sandy loam has a clay content of 11.1% and a sand content of 63.4%, loam has 19.7% clay and 40%

sand and Silt clay loam has a sand content of 7.6% and 33.2% clay (Carsel and Parrish 1988). Subsequently, these soil types will be referred to as sandy, loam, and clay, respectively to their clay content. The corresponding soil moisture retention curves and the hydraulic conductivities, both determined by the mentioned parameters, can be seen in Figure 4.

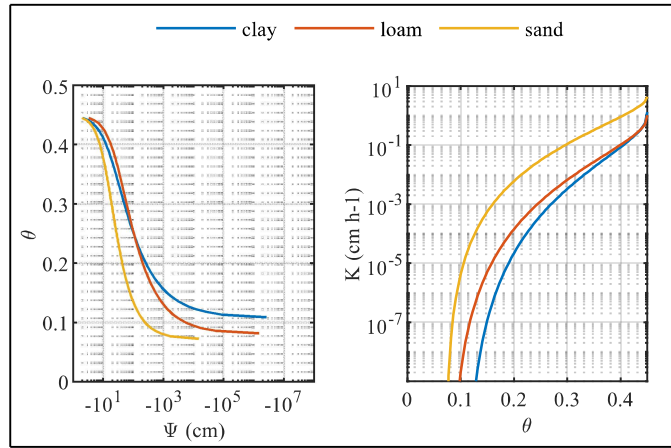


Figure 4 Soil moisture retention curves of the three soil types: clay, loam, and sand (left) and the hydraulic conductivity as a function of θ (right).

6.3.2 Hypothesis 2: Precipitation

Infiltration by rain is one of the key elements in defining the soil water profile. Therefore, an impact on the optimal root profile if the annual precipitation pattern changes was assumed. To test this hypothesis, five different precipitation scenarios were generated by manipulating the original rain input data. The five scenarios are as follows:

- 1) Original rain input data (R_0)
- 2) Original rain input reduced by 20% ($R_{-20\%}$)
- 3) Original rain input increased by 20% ($R_{+20\%}$)
- 4) Original rain input decreased during summer by 20%, rain during winter was then increased by 63% to match the original mean annual precipitation ($RS_{-20\%}$)
- 5) Original rain input decreased during winter by 20%, rain during summer was then increased by 6% to match the original mean annual precipitation ($RW_{-20\%}$)

Table 3 Precipitation of the five scenarios: R_0 , $R_{-20\%}$, $R_{+20\%}$, $RS_{-20\%}$, $RW_{-20\%}$. Separated according to mean annual precipitation, mean summer precipitation, and mean winter precipitation.

θ	R_0	$R_{-20\%}$	$R_{+20\%}$	$RS_{-20\%}$	$RW_{-20\%}$	Unit
Annual precipitation	782	629	939	782	782	mm
Summer precipitation	594	476	713	476	631	mm
Winter precipitation	188	150	225	305	150	mm

Mean annual precipitation (MAP) was 626 mm for $R_{-20\%}$, 782 mm for R_0 , $RS_{-20\%}$ and $RW_{-20\%}$, and 939 mm for $R_{+20\%}$. In summer, the precipitation ranges from 476 mm ($R_{-20\%}$, $RS_{-20\%}$) to 713 mm ($R_{+20\%}$) and in winter from 150 mm ($R_{-20\%}$, $RW_{-20\%}$) to 305 mm ($RS_{-20\%}$) (Table 3). Simulations were run in all three soil types: sand, loam, and clay.

6.3.3 Hypothesis 3: Temperature

To test the hypothesis, that increasing temperature and consequently higher potential evapotranspiration in the uppermost soil layer impact the optimal root profile, root profiles were tested in the period from 1979 to 1999 (P_{79}) and in the warmer period from 2000 to 2018 (P_{00}). Each dataset was run twice to simulate the root profiles over a period of 40-years. In P_{00} the mean temperature was 1°C , mean shortwave radiation was 5 W m^{-2} , and mean longwave radiation was 4 W m^{-2} higher compared to P_{79} , while MAP, mean relative humidity, and mean wind speed were approximately equal (Table 4). Simulations were again run in all three soil types: sand, loam, and clay.

Table 4 Mean of the climate input of the two climates before the year 2000 (P_{79}) and after (P_{00})

\varnothing	P_{79}	P_{00}	Unit
Air temperature	8.76	9.83	$^{\circ}\text{C}$
Shortwave radiation	112.9	118.3	W m^{-2}
Longwave radiation	310.5	314.1	W m^{-2}
Annual precipitation	783	782	mm
Summer precipitation	603	586	mm
Winter precipitation	180	196	mm
Relative humidity	80.9	80.7	%
Wind	3.8	3.7	m s^{-1}

6.4 Evaluation

The model was qualitatively evaluated by comparing the provided ORP's with observed root profiles in the literature. Deviations of observed root profiles with the ORP's of the model will be discussed and the plausibility of the model will be evaluated with general patterns of global root studies.

7 Results

The results of the simulations are shown in Figure 5-6 and Table 5-8. The annual transpiration T , the drought induced mortality M_Ψ and the net primary production NPP of the strategies simulated in a given setup were compared. Additionally, strategies were compared with the Efficiency-ratio (Eff) to compare the impact of the root profile on the strategy success, the strategy with the highest BM_{total} at the end of the simulation was defined as the ORP with $Eff=1$, ORP is equal to the strategy with the highest NPP.

7.1 Hypothesis 1: Soil

Across all soil types, strategies with shallow distributed root profiles showed comparable values for T . However, the strategy with the deepest tested root profile ($\beta=0.990$) transpired the most in sand with $T=694.9 \text{ mm yr}^{-1}$ and the least in clay with $T=449.0 \text{ mm yr}^{-1}$ compared to all strategies in all soil types (Table 5). In sand, strategies had consistently lower T -values with shallower root profiles, with the lowest T of the strategy with $\beta=0.920$ ($T=539.9 \text{ mm yr}^{-1}$). In the other soil types, strategies showed increasing T -values from the shallowest to deeper distributed profiles until a peak was reached, after which deeper distributed root profiles showed lower T -values again. In clay, the strategy with $\beta=0.951$ had the highest T with 554.1 mm yr^{-1} , and the strategy with $\beta=0.978$ had the highest T in loam with 637.5 mm yr^{-1} (Figure 5a).

Drought induced mortality M_Ψ across all soil types was the highest for strategies with $\beta=0.920$. In sand and loam, strategies showed lower M_Ψ -values consistently with deeper distributed root profiles, ranging from 6.5 to 37.5 g yr^{-1} per kg total biomass in sand and 9.1 to $36.5 \text{ g kg}^{-1} \text{ yr}^{-1}$ in loam (Table 5). This consistency was not true for strategies tested in clay, where strategies with $\beta=0.920$ also showed the highest values for M_Ψ , and the lowest with $\beta=0.990$

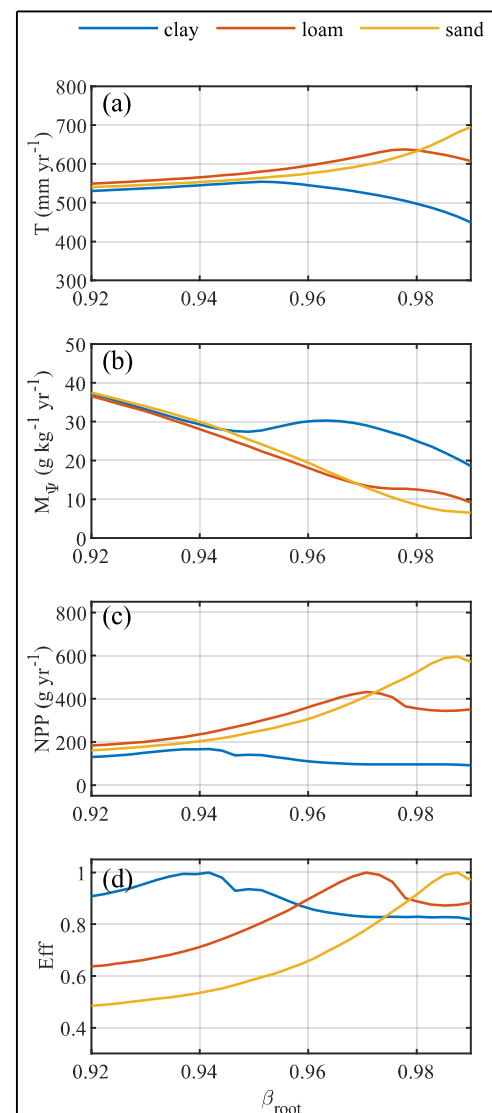


Figure 5 Model output of the three soil types; (a) mean annual transpiration (b) drought induced mortality (c) net primary production and (d) efficiency, all displayed vs. the root distribution index beta.

(18.6-37.2 g kg⁻¹ yr⁻¹) (Table 5). Yet, strategies in clay with β -values between 0.949 and 0.961 showed within this range higher values for M_{Ψ} with deeper distributed root profiles (Figure 5b). Although the strategies tested in loam and sand consistently showed lower values for M_{Ψ} with deeper root profiles compared to profiles in clay, the effect between deeper root profiles was smaller (Figure 5b).

Table 5 Minimum and maximum values of the model output of the three soil types: mean annual transpiration, drought induced mortality, net primary production, and efficiency; with the associated root distribution index β .

	clay		loam		sand		Unit
	min. value	max. value	min. value	max. value	min. value	max. value	
T	449.0 ($\beta=0.990$)	554.1 ($\beta=0.951$)	549.4 ($\beta=0.920$)	637.5 ($\beta=0.978$)	539.9 ($\beta=0.920$)	694.9 ($\beta=0.990$)	mm yr ⁻¹
M_{Ψ}	18.6 ($\beta=0.990$)	37.2 ($\beta=0.920$)	9.1 ($\beta=0.990$)	36.5 ($\beta=0.920$)	6.5 ($\beta=0.990$)	37.5 ($\beta=0.920$)	g kg ⁻¹ yr ⁻¹
NPP	91.7 ($\beta=0.990$)	167.6 ($\beta=0.942$)	183.9 ($\beta=0.920$)	431.4 ($\beta=0.971$)	160.7 ($\beta=0.920$)	596.6 ($\beta=0.988$)	g yr ⁻¹
Eff	0.82 ($\beta=0.990$)	1 ($\beta=0.942$)	0.64 ($\beta=0.920$)	1 ($\beta=0.971$)	0.49 ($\beta=0.920$)	1 ($\beta=0.988$)	

Highest NPP-values, across all soil types, had strategies with deep root profiles in sand, with the highest NPP of 596.6 g yr⁻¹ for the strategy with $\beta=0.988$. While shallower root profiles tested in loam had higher NPP-values, compared to shallow profiles in the other soils (Figure 5c). In loam, the highest NPP was 431.4 g yr⁻¹ for the strategy with $\beta=0.971$. Strategies tested in clay, showed overall the lowest values for NPP, ranging from 91.7 g yr⁻¹ with $\beta=0.990$ to 167.6 g yr⁻¹ with $\beta=0.942$. The lowest NPP in loam and sand had the strategies with $\beta=0.920$, with 183.9 g yr⁻¹ and 160.7 g yr⁻¹, respectively (Table 5).

In sand, the strategy with the ORP ($\beta=0.988$) had 50% of their root biomass in the first 57.4 cm of the soil column and had a BM_{total} of 33.9 kg at the end of the simulation. The least effective profile in sand ($\beta=0.92$) could only reach 46% of the optimum. In loam, the strategy with the ORP ($\beta=0.971$) had 50% of their root biomass in the upmost 24.5 cm of the soil column and had a BM_{total} of 27.3 kg at the end of the simulation. The least effective root profile in loam ($\beta=0.920$) could only reach 64% of the optimum. And in clay, the strategy with the ORP ($\beta=0.942$) had 50% of their root biomass in first 11.6 cm of the soil and had a BM_{total} of 16.7 kg at the end of the simulation. The least effective root profile in clay ($\beta=0.990$) could only reach 82% of the optimum (Figure 5d).

7.2 Hypothesis 2: Precipitation

Strategies were simulated in the scenarios R_{-20%}, R_{+20%}, RS_{-20%} and RW_{-20%} and were compared within a soil with the results of the base scenario R₀ (equal to the results of H1).

In the scenario R-20% annual precipitation was reduced by 20%. T was lower for all strategies across all soil types in the R-20% scenario (Figure 6a-c). The strategies with the highest T-values within a soil had shallower distributed root profiles compared to the strategies in R₀, with $\beta=0.947$ in clay, $\beta=0.968$ in loam and $\beta=0.985$ in sand (Table 6). The general pattern of M_{Ψ} did not change. Strategies in all soil types with $\beta=0.920$ had the highest and with $\beta=0.99$ the lowest values of M_{Ψ} . However, M_{Ψ} was consistently higher for all root profiles in all soils in the R-20% scenario (Figure 6d-f). Across all soil types, all strategies had lower NPP-values with reduced MAP (Figure 6g-i). Strategies with the highest values for NPP in the R-20% scenario had shallower distributed root profiles across all soil types with $\beta=0.932$ in clay, $\beta=0.961$ in loam and $\beta=0.980$ in sand (Table 6). No clear pattern could be found in the efficiency difference of the least effective profile compared to the ORP. Eff for the least effective profile was 0.82 in clay and equal compared to the R₀ scenario. While in loam Eff was slightly higher with 0.66 and lower in sand with Eff=0.44, both compared to Eff of the R₀ scenario (Figure 6j-l).

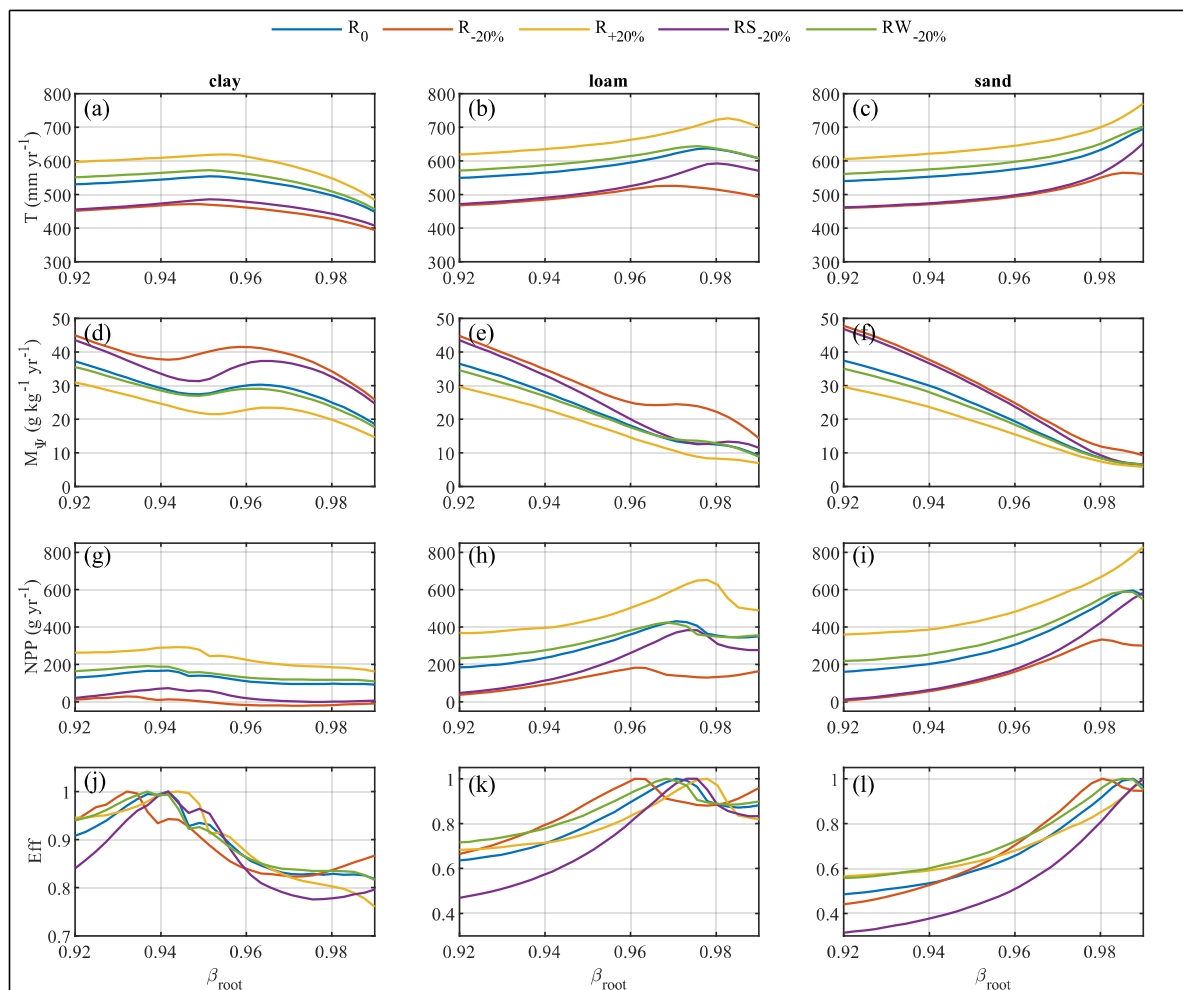


Figure 6 Model output of the three soil types under the five precipitation scenarios (R₀, R-20%, R+20%, RS-20%, RW-20%); (a-c) mean annual transpiration (d-f) drought induced mortality (g-i) net primary production and (j-k) efficiency, all displayed vs. the root distribution index β .

In the $R_{+20\%}$ scenario with increased MAP, strategies showed an opposite pattern. M_{Ψ} was consistently lower across all soil types of all strategies compared to the R_0 scenario (Figure 6d-f), while strategies with the highest and the lowest values for M_{Ψ} still had a root profile of $\beta=0.920$ and $\beta=0.990$, respectively (Table 6). T was consistently higher, while the strategies with the highest T-values tested in the $R_{+20\%}$ scenario had deeper root profiles in clay with $\beta=0.953$ and in loam with $\beta=0.983$ (Figure 6a-c). In sand, the strategy with the highest T-value had the deepest tested profile ($\beta=0.990$) and was equal to the profile with the highest T in the R_0 scenario (Table 6). NPP of all strategies was also higher across all soil types with the highest values of NPP for the strategies with $\beta=0.944$ in clay, $\beta=0.978$ in loam and $\beta=0.990$ in sand (Figure 6g-i). Therefore, the ORP's were deeper distributed in the $R_{+20\%}$ scenario compared to the ORP's in the R_0 scenario across all soil types. No clear pattern could be seen in the efficiency ratio between the ORP and the least effective strategy (Figure 6j-l). The least effective strategy in clay could only reach 76% of the ORPs BM_{total} and was lower compared to Eff of R_0 . In loam and sand the least effective strategy reached 68% and 57%, respectively, of the ORP's BM_{total} , which was higher compared to Eff of R_0 (Table 6).

Table 6 Minimum and maximum values of the model output of the three soil types under the five precipitation scenarios (R_0 , $R_{-20\%}$, $R_{+20\%}$, $RS_{-20\%}$, $RW_{-20\%}$): mean annual transpiration, drought induced mortality, net primary production, and efficiency; with the associated root distribution index β .

	R_0		$R_{-20\%}$		$R_{+20\%}$		$RS_{-20\%}$		$RW_{-20\%}$		
	min. value	max. value	min. value	max. value	min. value	max. value	min. value	max. value	min. value	max. value	Unit
clay											
T	449.0 ($\beta=0.990$)	554.1 ($\beta=0.951$)	394.4 ($\beta=0.990$)	472.0 ($\beta=0.947$)	483.9 ($\beta=0.990$)	619.4 ($\beta=0.954$)	408.0 ($\beta=0.990$)	485.8 ($\beta=0.951$)	556.5 ($\beta=0.990$)	572.2 ($\beta=0.951$)	mm yr ⁻¹
M_{Ψ}	18.6 ($\beta=0.990$)	37.2 ($\beta=0.920$)	25.8 ($\beta=0.990$)	44.9 ($\beta=0.920$)	14.7 ($\beta=0.990$)	31.0 ($\beta=0.920$)	24.7 ($\beta=0.990$)	43.5 ($\beta=0.920$)	17.6 ($\beta=0.990$)	35.5 ($\beta=0.920$)	g kg ⁻¹ yr ⁻¹
NPP	91.7 ($\beta=0.990$)	167.6 ($\beta=0.942$)	-21.0 ($\beta=0.971$)	28.2 ($\beta=0.932$)	162.5 ($\beta=0.990$)	292.3 ($\beta=0.944$)	0.04 ($\beta=0.976$)	72.2 ($\beta=0.942$)	109.9 ($\beta=0.990$)	190.9 ($\beta=0.937$)	g yr ⁻¹
Eff	0.82 ($\beta=0.990$)	1 ($\beta=0.942$)	0.82 ($\beta=0.971$)	1 ($\beta=0.932$)	0.76 ($\beta=0.990$)	1 ($\beta=0.944$)	0.78 ($\beta=0.976$)	1 ($\beta=0.942$)	0.82 ($\beta=0.990$)	1 ($\beta=0.937$)	
loam											
T	549.4 ($\beta=0.920$)	637.5 ($\beta=0.978$)	467.8 ($\beta=0.920$)	526.0 ($\beta=0.968$)	618.9 ($\beta=0.920$)	727.3 ($\beta=0.983$)	471.7 ($\beta=0.920$)	593.0 ($\beta=0.980$)	571.4 ($\beta=0.920$)	643.7 ($\beta=0.976$)	mm yr ⁻¹
M_{Ψ}	9.1 ($\beta=0.990$)	36.5 ($\beta=0.920$)	14.4 ($\beta=0.990$)	44.7 ($\beta=0.920$)	7.0 ($\beta=0.990$)	29.6 ($\beta=0.920$)	11.5 ($\beta=0.990$)	43.5 ($\beta=0.920$)	8.9 ($\beta=0.990$)	34.6 ($\beta=0.920$)	g kg ⁻¹ yr ⁻¹
NPP	183.9 ($\beta=0.920$)	431.4 ($\beta=0.971$)	37.1 ($\beta=0.920$)	182.1 ($\beta=0.961$)	367.6 ($\beta=0.920$)	652.7 ($\beta=0.978$)	47.0 ($\beta=0.920$)	383.0 ($\beta=0.976$)	233.2 ($\beta=0.920$)	424.4 ($\beta=0.968$)	g yr ⁻¹
Eff	0.64 ($\beta=0.920$)	1 ($\beta=0.971$)	0.66 ($\beta=0.920$)	1 ($\beta=0.961$)	0.68 ($\beta=0.920$)	1 ($\beta=0.978$)	0.47 ($\beta=0.920$)	1 ($\beta=0.976$)	0.72 ($\beta=0.920$)	1 ($\beta=0.968$)	
sand											
T	539.9 ($\beta=0.920$)	694.9 ($\beta=0.990$)	459.8 ($\beta=0.920$)	564.6 ($\beta=0.985$)	605.7 ($\beta=0.920$)	771.1 ($\beta=0.990$)	462.0 ($\beta=0.920$)	652.1 ($\beta=0.990$)	561.4 ($\beta=0.920$)	700.7 ($\beta=0.990$)	mm yr ⁻¹
M_{Ψ}	6.5 ($\beta=0.990$)	37.5 ($\beta=0.920$)	9.2 ($\beta=0.990$)	47.8 ($\beta=0.920$)	5.9 ($\beta=0.990$)	29.6 ($\beta=0.920$)	6.6 ($\beta=0.990$)	46.8 ($\beta=0.920$)	6.5 ($\beta=0.990$)	35.1 ($\beta=0.920$)	g kg ⁻¹ yr ⁻¹
NPP	160.7 ($\beta=0.920$)	596.6 ($\beta=0.988$)	6.6 ($\beta=0.920$)	332.8 ($\beta=0.980$)	359.7 ($\beta=0.920$)	827.9 ($\beta=0.990$)	11.3 ($\beta=0.920$)	583.6 ($\beta=0.990$)	218.3 ($\beta=0.920$)	589.2 ($\beta=0.985$)	g yr ⁻¹
Eff	0.49 ($\beta=0.920$)	1 ($\beta=0.988$)	0.44 ($\beta=0.920$)	1 ($\beta=0.980$)	0.57 ($\beta=0.920$)	1 ($\beta=0.990$)	0.31 ($\beta=0.920$)	1 ($\beta=0.990$)	0.56 ($\beta=0.920$)	1 ($\beta=0.985$)	

In the RS-20% scenario, precipitation was reduced during summer by 20% and increased in winter to achieve the same MAP as in R_0 . In this scenario, all tested strategies had lower T-values across all soil types, while for shallow root profiles T-values were comparable to the T-values of the $R_{-20\%}$ scenario (Figure 6a-c). However, strategies with the highest T had equal root profiles in clay and sand compared to R_0 with $\beta=0.951$ and $\beta=0.990$ respectively (Table 6). In loam, the root profile with the highest T was slightly deeper distributed with $\beta=0.980$, than the strategy with the highest T in the R_0 scenario (Table 6). M_Ψ showed the same pattern across all soil types, where the shallowest profiles ($\beta=0.920$) had the highest M_Ψ , and the deepest profiles ($\beta=0.990$) had the lowest M_Ψ (Table 6). Although, M_Ψ was in general higher in the RS-20% scenario, for deep root profiles in loam and sand values were comparable with the M_Ψ -values of deep root strategies in R_0 (Figure 6d-f). NPP was lower in all strategies across all soil types, only the strategy with $\beta=0.99$ in sand had a higher NPP than the NPP of this strategy tested in scenario R_0 (Figure 6i). This strategy had also the ORP for the RS-20% scenario in sand and had therefore a deeper distributed ORP compared to the ORP in sand in scenario R_0 (Table 6). In loam, the ORP was also deeper distributed with $\beta=0.976$ (Figure 6k). While in clay, ORPs were equal in the scenarios RS-20% and R_0 (Table 6). It is noticeable that the range between the ORPs and the least effective root profiles increased in all soils, with Eff-values for the least effective profiles of 0.78 in clay, 0.47 in loam and 0.31 in sand. Although, this effect was larger in loam and sand (Figure 6j-l).

Winter precipitation was reduced by 20% in the RW-20% scenario and increased in summer to achieve the same annual precipitation as in the R_0 scenario. Strategies tested in the RW-20% scenario showed the smallest deviations to strategies in the R_0 scenario, compared to the other three scenarios (Figure 6). However, compared with R_0 , T was higher for all strategies across all soil types with slightly decreasing effect size for strategies with deep distributed root profiles (Figure 6a-c). Strategies with the highest T were equal in clay and sand with those in R_0 , with $\beta=0.951$ in clay and $\beta=0.990$ in sand (Table 6). In loam, the strategy with the highest T were slightly deeper distributed with $\beta=0.976$ (Table 6). In the RW-20% scenario, strategies with the highest and lowest M_Ψ were the same in all soils and were consistent with the other scenarios, with $\beta=0.920$ and $\beta=0.990$ respectively (Table 6). M_Ψ was in the majority of the strategies lower in the RW-20% scenario than in R_0 , with the exception of strategies with β between 0.968 and 0.983 in loam where strategies showed slightly higher M_Ψ -values (Figure 6d-f). Furthermore, in sand, strategies with profiles deeper distributed than $\beta=0.985$ showed M_Ψ -values equal to those in the R_0 scenario (Figure 6f). In clay, all strategies had a higher NPP, with the highest NPP for the strategy with $\beta=0.937$ (Figure 6g). In loam and sand, strategies with the highest

NPP had root profiles with $\beta=0.968$ in loam and $\beta=0.985$ in sand (Table 6). The ORP's in the RW-20% scenario were therefore deeper distributed in all soil types (Figure 6j-l). The least effective strategies had an equal Eff-value of 0.82 in clay and higher Eff-values of 0.72 in loam and 0.56 in sand compared to the Eff-values of the least effective strategies in the R_0 scenario (Table 6).

7.3 Hypothesis 3: Temperature

Strategies were tested with two different climates and were compared within a soil type. The P_{79} climate includes the years 1979 to 1999 and the P_{00} climate includes the years 2000 to 2018. The differences, such as temperature, precipitation, and radiation of these two periods are listed in table 4. The annual PET in the P_{79} climate was $1252.5 \text{ mm yr}^{-1}$ and marginally below the annual PET of $1255.1 \text{ mm yr}^{-1}$ in the P_{00} climate. During summer when strategies were active, the mean PET with $1187.4 \text{ mm yr}^{-1}$ in the P_{00} climate was higher than the $1161.2 \text{ mm yr}^{-1}$ in the P_{79} climate (Table 7).

Table 7 Potential evapotranspiration and the potential evapotranspiration during summer of the two climate scenarios

	P_{79}	P_{00}	Unit
PET	1252.5	1255.1	mm yr^{-1}
PET(summer)	1161.2	1187.4	mm yr^{-1}

However, strategies tested in both climates showed only small differences in their T (Figure 7a-c). In sand, T was lower for all strategies under the P_{00} climate, while in both climates the strategy with $\beta=0.99$ had the highest T-values. While in clay and loam, strategies with the highest T differ between the two climates and had slightly deeper distributed root profiles under P_{00} . In clay, under P_{79} , the strategy with $\beta=0.944$ and under P_{00} the strategy with $\beta=0.947$ had the highest T (Table 8). In loam, the strategy with the highest T had a β of 0.973 under P_{79} and a β of 0.976 under P_{00} (Table 8). The general pattern of M_Ψ was also the case in this setting, with the highest M_Ψ for the shallowest root profile ($\beta=0.920$) and the lowest M_Ψ for the deepest root profile ($\beta=0.990$) in all soil types (Table 8). In sand and clay, M_Ψ was consistently higher under P_{00} (Figure 7e-f). While in clay, strategies with deeper distributed profiles had lower values for M_Ψ under P_{00} (Figure 7d). Under the P_{00} climate, NPP was lower for all strategies across all soil types, with one exception the strategy with the highest NPP in clay with $\beta=0.935$ (Figure 7g-i). The strategies with $\beta=0.971$ in loam and with $\beta=0.988$ in sand had the highest NPP under P_{00} (Table 8). Under P_{79} , highest NPP showed the strategies with $\beta=0.922$ in clay, $\beta=0.66$ in loam and $\beta=0.988$ in sand (Table 8). Therefore, the ORP's were deeper distributed in clay and loam under the P_{00} climate compared with the P_{79} climate, in sand the ORP's were equal for both climates. The efficiency of the least effective strategies was slightly lower in all soils under the P_{00} climate compared with P_{79} climate (Figure 7j-l).

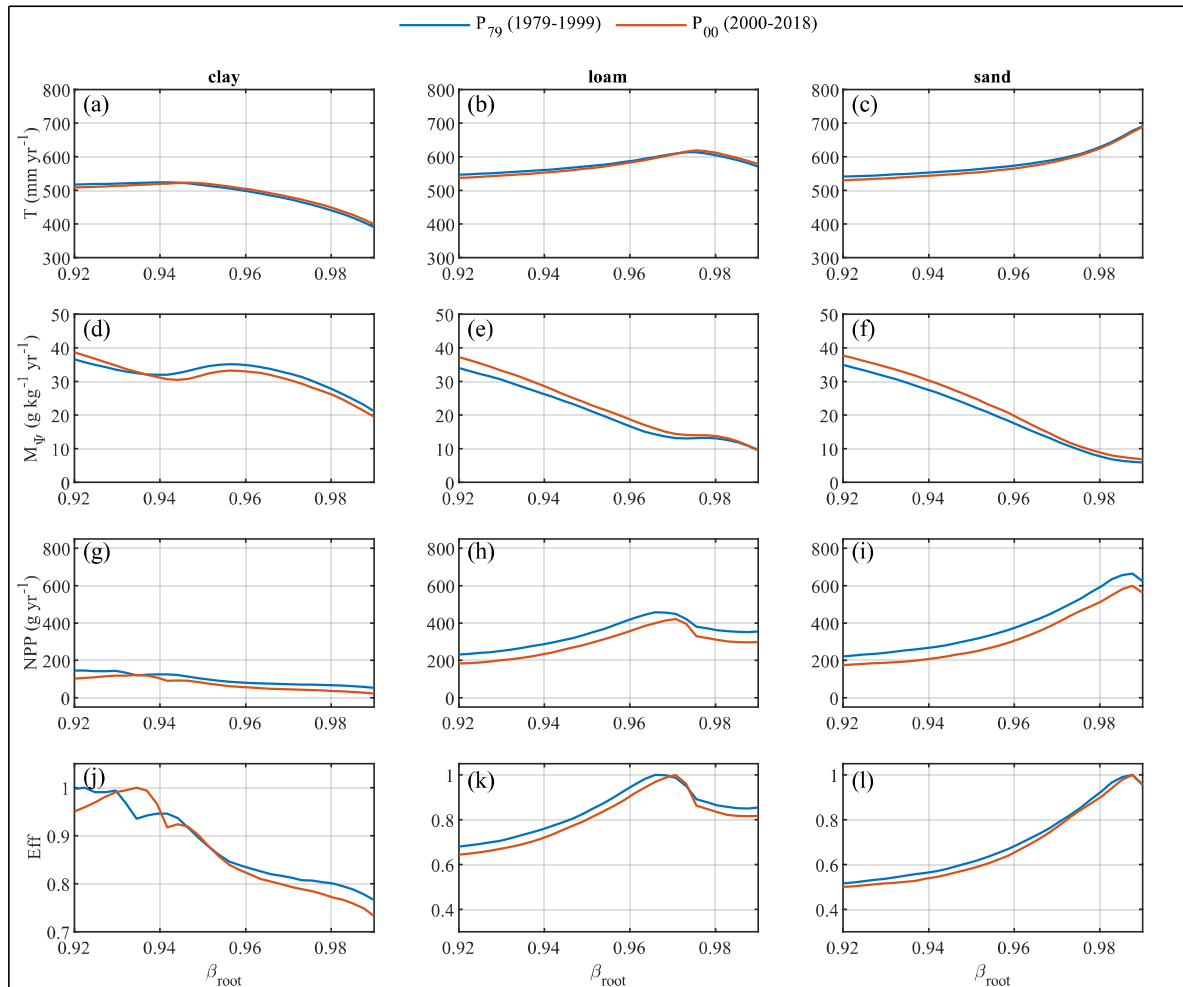


Figure 7 Model output of the three soil types under the two climate scenarios (P_{79} and P_{00}); (a-c) mean annual transpiration (d-f) drought induced mortality (g-i) net primary production and (j-k) efficiency, all displayed vs. the root distribution index β .

Table 8 Minimum and maximum values of the model output of the three soil types under the two climate scenarios (P_{79} and P_{00}): mean annual transpiration, drought induced mortality, net primary production, and efficiency; with the associated root distribution index β .

	P_{79}		P_{00}		
	min. value	max. value	min. value	max. value	Unit
clay					
T	390.6 ($\beta=0.990$)	523.6 ($\beta=0.944$)	399.1 ($\beta=0.990$)	522.8 ($\beta=0.947$)	mm yr ⁻¹
Mψ	21.2 ($\beta=0.990$)	36.6 ($\beta=0.920$)	19.5 ($\beta=0.990$)	38.7 ($\beta=0.920$)	g kg ⁻¹ yr ⁻¹
NPP	53.6 ($\beta=0.990$)	146.3 ($\beta=0.922$)	21.8 ($\beta=0.990$)	121.1 ($\beta=0.935$)	g yr ⁻¹
Eff	0.77 ($\beta=0.990$)	1 ($\beta=0.922$)	0.73 ($\beta=0.990$)	1 ($\beta=0.935$)	
loam					
T	546.8 ($\beta=0.920$)	613.4 ($\beta=0.973$)	537.4 ($\beta=0.920$)	619.7 ($\beta=0.976$)	mm yr ⁻¹
Mψ	9.5 ($\beta=0.990$)	34.0 ($\beta=0.920$)	9.6 ($\beta=0.990$)	37.2 ($\beta=0.920$)	g kg ⁻¹ yr ⁻¹
NPP	231.5 ($\beta=0.920$)	457.4 ($\beta=0.966$)	182.7 ($\beta=0.920$)	421.6 ($\beta=0.971$)	g yr ⁻¹

Eff	0.68 ($\beta=0.990$)	1 ($\beta=0.966$)	0.64 ($\beta=0.920$)	1 ($\beta=0.971$)	
sand					
T	540.7 ($\beta=0.920$)	690.4 ($\beta=0.990$)	529.9 ($\beta=0.920$)	689.0 ($\beta=0.990$)	mm yr ⁻¹
M_ψ	5.9 ($\beta=0.990$)	35.0 ($\beta=0.920$)	6.8 ($\beta=0.990$)	37.8 ($\beta=0.920$)	g kg ⁻¹ yr ⁻¹
NPP	221.9 ($\beta=0.920$)	664.8 ($\beta=0.988$)	174.3 ($\beta=0.920$)	599.1 ($\beta=0.988$)	g yr ⁻¹
Eff	0.52 ($\beta=0.920$)	1 ($\beta=0.988$)	0.50 ($\beta=0.920$)	1 ($\beta=0.988$)	

7.4 Sensitivity analysis

A sensitivity analysis was performed to identify the impact of parameters on the ORP's. In total, 16 parameters were tested with a value higher and lower as the value used in the model (Table 9).

Table 9 Parameters that were considered in the sensitivity analysis with the associated β of the ORP with high and low values

Description	Symbol	Sens. Analy. Low value	Value	Sens. Analy. High value	Unit
General parameters					
Fraction parameter for PET	σ	0.3 ($\beta=0.965$)	0.4 ($\beta=0.965$)	0.5 ($\beta=0.965$)	
Plant parameters					
Tree height	h	5 ($\beta=0.965$)	20 ($\beta=0.965$)	40 ($\beta=0.965$)	m
Maximum rooting depth	z_{max}	3 ($\beta=0.965$)	4 ($\beta=0.65$)	4.5 ($\beta=0.65$)	m
Leaf area index	LAI	2 ($\beta=0.970$)	4 ($\beta=0.965$)	6 ($\beta=0.960$)	m ² m ⁻²
Fine root biomass	BM_{root}	200 ($\beta=0.990$)	400 ($\beta=0.965$)	600 ($\beta=0.965$)	g
Mean fine root radius	r_r	0.01 ($\beta=0.965$)	0.29 ($\beta=0.965$)	0.6 ($\beta=0.965$)	mm
Root resistivity	R_r^*	20 ($\beta=0.965$)	25 ($\beta=0.965$)	30 ($\beta=0.965$)	MPa s g mmol ⁻¹
Specific root length	r_l	5 ($\beta=0.965$)	12.2 ($\beta=0.965$)	20 ($\beta=0.965$)	m g ⁻¹
Stem-to-leaf specific hydr. conductivity	K_a	2 ($\beta=0.965$)	4 ($\beta=0.965$)	6 ($\beta=0.965$)	mmol LAI ⁻¹ s ⁻¹ MPa ⁻¹
Photosynthesis					
Max. Carboxylation rate	v_{cmax25}	40 ($\beta=0.965$)	60 ($\beta=0.965$)	80 ($\beta=0.965$)	μmol mol ⁻¹
Stomata					
Max. stomata conductance	g_{sw}	0.2 ($\beta=0.965$)	0.4 ($\beta=0.965$)	0.8 ($\beta=0.965$)	mol m ⁻² s ⁻¹
Water potentials					
Water potential at which $\beta_{wet}=1$	ψ_{opt}	-0.01 ($\beta=0.965$)	-0.05 ($\beta=0.965$)	-0.5 ($\beta=0.965$)	MPa
50% loss of conductivity	ψ_{50}	-3.1 ($\beta=0.965$)	-3.5 ($\beta=0.965$)	-3.9 ($\beta=0.965$)	MPa
12% loss of conductivity	$\psi_{leaf,min}$	-1.7 ($\beta=0.965$)	-2.1 ($\beta=0.965$)	-2.5 ($\beta=0.965$)	MPa
Carbon balance					
Background mortality	M_b	0 ($\beta=0.965$)	0.01 ($\beta=0.965$)	0.1 ($\beta=0.965$)	g g ⁻¹ yr ⁻¹
Drought induced mortality	M_ψ	0.3 ($\beta=0.965$)	0.5 ($\beta=0.965$)	0.7 ($\beta=0.965$)	g g ⁻¹ yr ⁻¹

Only two of these 16 parameters impacted the ORP in loamy soil after a 20-year period, namely LAI and BM_{root} . In the model, LAI was set to $4 \text{ m}^2 \text{ m}^{-2}$, for the sensitivity analysis a reduced LAI of $2 \text{ m}^2 \text{ m}^{-2}$ and an increased LAI of $6 \text{ m}^2 \text{ m}^{-2}$ were tested. The ORP was deeper distributed for a reduced LAI ($\beta=0.970$) and shallower distributed with an increased LAI ($\beta=0.960$).

A fine root biomass of 400 g m^{-2} was used in the model, for the sensitivity analyses a lower BM_{root} of 200 g m^{-2} and a higher BM_{root} of 600 g m^{-2} was tested. Although there was no change in the ORP for a higher BM_{root} ($\beta=0.965$), a lower BM_{root} shifted the ORP to the deepest root profile tested with $\beta=0.99$ (Table 9). Strategies with a reduced LAI, had lower values for M_{Ψ} , because of a reduced transpiration and therefore in general lower values for Ψ_{leaf} , which reduces the risk of cavitation (Figure 8). In addition, they had lower turnover rates, due to a reduced BM_{leaf} . However, a reduced LAI leads to a lower NPP, because of the reduced assimilation rate (Figure 8). For BM_{root} an opposite effect was observed, with an increase M_{Ψ} with lower BM_{root} , because of the limited water supply and therefore higher values for Ψ_{leaf} and an increased risk for cavitation. Still, strategies with a lower BM_{root} had higher NPP's because of the reduced turnover rate (TO_{root}) (Figure 8).

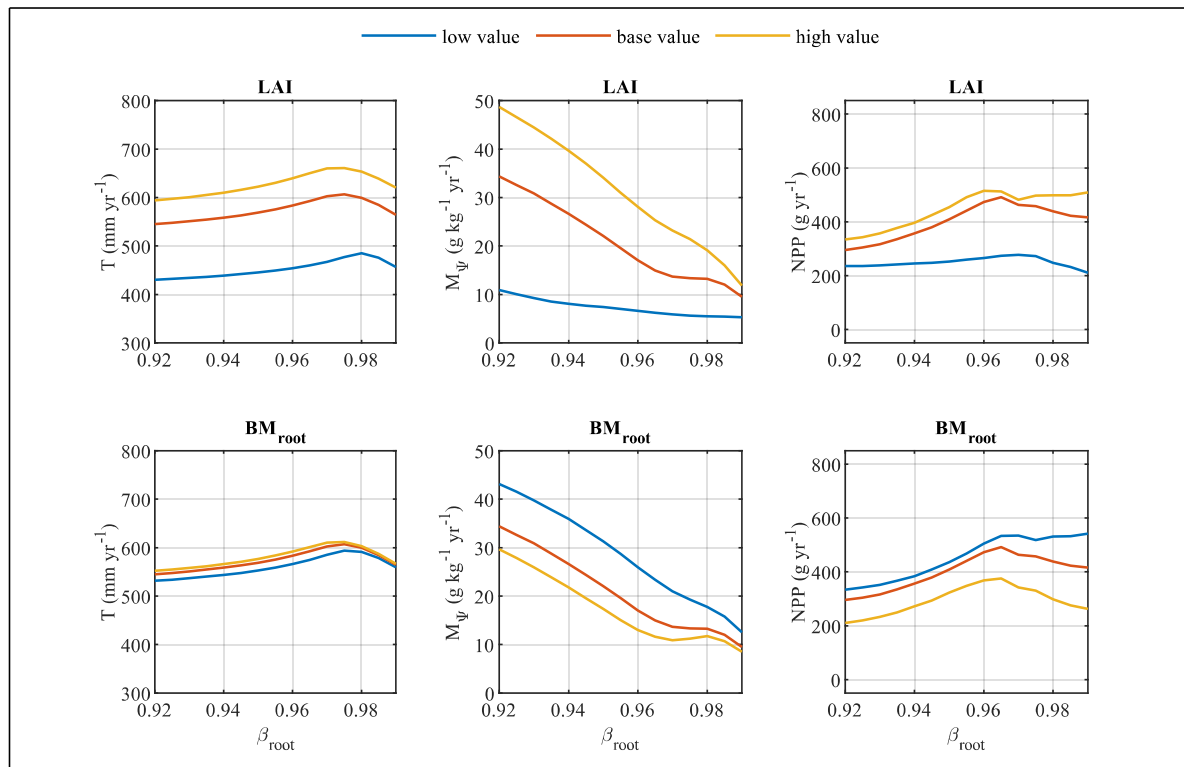


Figure 8 Model output of the parameters LAI and BM_{root} of the sensitivity analysis; Low, base, and high values are shown in table 9.

The ORP's provided from the model were not really sensitive to the tested parameters, except of LAI and BM_{root} . However, most of the parameters had an impact on other aspects of the model, such as NPP, M_{Ψ} and T (Section 11.2). Noteworthy was the effect of the specific root

length (r_l), where strategies with a lower r_l had lower T and higher M_Ψ values (Figure 15). Besides, the mortality rates (M_b , M_Ψ), Ψ_{50} , tree height (h) and v_{cmax25} , the specific root length was the parameter with the highest impact on the NPP without affecting the ORP.

8 Discussion

In this study the optimal root profiles for different environmental conditions were determined by using a process-based model. The results show clear evidence, that the establishment of a suitable root profile is crucial for the success of trees and that different environmental conditions play a major role in that aspect. The following discussion is structured in seven sections. The first three sections discuss the impact of environmental conditions to the ORP, namely soil texture, precipitation, and temperature. In the fourth, fifth and sixth section the sensitivity analyses, limitations, and the evaluation of the here presented model will be discussed. The last section summarizes the findings of this study.

8.1 Optimal root profile and soil texture

Overall, the soil texture had the largest effect on the ORP's. As expected, the ORP was the shallowest in fine textured soil compared to the ORP's in more coarser soils (Figure 9). The ORP in loamy soil (19.2% clay) had a β of 0.971 and 50% of BM_{root} in the first 24.5 cm of the soil and was shallower distributed in the clay soil (33.2% clay) with 50% of BM_{root} in the first 11.6 cm ($\beta=0.942$). In sandy soil (11.1% clay), the ORP was the deepest distributed with 50% of BM_{root} in the first 57.4 cm ($\beta=0.988$). The mean distribution of the three ORP's was $\beta=0.967$, which is not really representative due to the small number of soils tested. Nevertheless, it agrees perfectly with the mean root distribution of temperate deciduous forests with a β of 0.966 (Jackson et al. 1996).

Because of the high diversity of soil types and local climatic and stand conditions, it is challenging to compare the provided root distributions of the model with observed root profiles. For instance, a study that investigated the root profiles of *Robinia pseudoacacia* (L.) in different soils found a with the model comparable root distribution for loamy soil with 50% of BM_{root} in the first 26.8-31.4 cm in a soil containing 15.0-17.6% clay (Chang et al. 2012).

Contrary to the assumptions of the authors and the results of this study, roots were similar distributed in the soil with the higher clay content (34.3-35.5%). This is explained with

stand characteristics such as higher belowground competition because of a greater tree density and in general larger trees at the site with more clay content (Chang et al. 2012). Further, the root profiles of oak stands in north Germany were shallower in sand and silt than in loam and

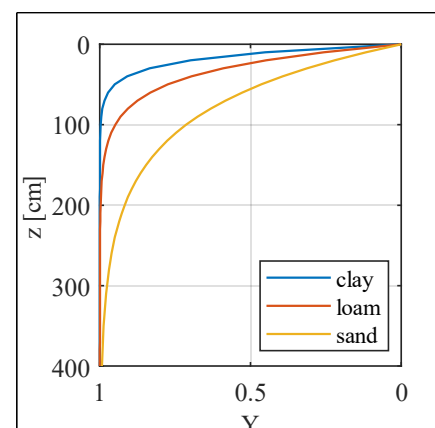


Figure 9 Optimal root profiles of H1; Cumulative root distribution as a function of beta. clay: $\beta=0.942$, loam: $\beta=0.971$, sand: $\beta=0.988$.

clay. In the study, it was hypothesized that root profiles under the climatic conditions of Central Europe are more influenced by nutrient availability than by water availability (Thomas 2000). The root profiles in this study were investigated in the year 1993, before the occurrence of more intense drought scenarios in Europe (Grillakis 2019), which could potentially declare this assumption outdated. Nonetheless, by comparing the provided root profiles of H3 under the climate conditions from 1979 to 1999, they still present a contrasting pattern to the findings of Thomas (2000). This is because of the model design, which assumed water as the limiting factor and provided the ORP in terms of maximum carbon uptake while avoiding cavitation, even if water is not limited. However, in water limited ecosystems observed root profiles should adapt to the soil moisture conditions. Such as, in a semi-arid climate, *Haloxylon ammodendron* (C.A. Mey) a small xeric tree, had significant deeper roots in sandy soil compared to roots of the same species in more heavy textured soil (Xu and Li 2008). In summary, this underlines the complexity of identifying the optimal root profile under different environmental conditions. Despite this, the provided pattern by the here presented model is in coincident with the findings of global root studies, where rooting depth of several vegetation types correlates not only, but also with soil texture (Schenk and Jackson 2002; Fan et al. 2017). Which makes the model output plausible. Although, this effect seems to be weaker on a global scale, as the varying water table depths can influence rooting depth by pushing roots into a shallower profile to avoid oxygen stress, or by pulling roots downwards to reach deeper water reservoirs (Fan et al. 2017). However, in this study, root profiles were limited in their rooting depth to avoid access to the water table and to exclude this disturbing effect. Consequently, within the model, root profiles had only access to water infiltrated into the soil by precipitation. In coarse soils, water infiltrates faster and therefore deeper, due to their higher hydraulic conductivity (Figure 4). In coarse soils, deep roots have therefore more access to water, which would otherwise be lost through drainage. The transpiration rate of strategies increased in all soils from shallow root profiles to deeper distributed root profiles until a maximum transpiration rate is reached. The maximum transpiration rate within a soil was reached by a shallower root profile in clay ($\beta=0.952$) compared with loam, where a root profile with $\beta=0.978$ had the highest transpiration rate. In sand, the deepest tested root profile ($\beta=0.99$) had the highest transpiration rate. The decreasing transpiration rates for root profiles deeper distributed than the mentioned profiles indicate the different infiltration profiles of the tested soils. These results agree with previously published similar model approaches (e.g., Collins & Bras, 2007a; Rudd et al., 2014). Transpiration rate is linked with the stomata conductance and therefore correlates strongly with the carbon assimilation rate. Consequently, the root profile with the highest transpiration rate is often

defined as the optimal root profile, especially in water limited ecosystems, such as in the work of Collins & Bras (2007) and Rudd et al. (2014). The ORP's in this study are defined as the profiles with the highest NPP, which includes a drought induced mortality rate (M_Ψ).

Because of the model approach, that root profiles do not dynamically adapt to soil water conditions, M_Ψ can be divided in two sections. First, increased M_Ψ for roots in the topsoil, due to soil evaporation and second increasing M_Ψ , due to roots located below the infiltration depth. The upmost soil layers loose water through evaporation, RWU and drainage and are more likely to reach lower values for Ψ_{soil} than deeper soil layers. Deeper soil layers only loose water through drainage and RWU and are unlikely to reach the same values for Ψ_{soil} because roots are only capable of absorbing water if Ψ_{soil} is above Ψ_{wp} . This leads to the highest M_Ψ for shallow root profiles and decreasing M_Ψ for deeper profiles, due to the lower proportion of roots in the first soil layers. This decrease is consistent until deeper root profiles are distributed below the infiltration profile, which leads again to an increase of M_Ψ . With root profiles increasingly deeper distributed, the proportion of roots in the first soil layers decreases and explains why M_Ψ was not increasing consistently with deeper roots (Figure 5b). This effect was observed in all soils, but was most pronounced in clay, due to the lowest infiltration depth. However, the implementation of M_Ψ resulted in shallower ORP's than the root profiles with the highest transpiration rate. Although, the here presented M_Ψ is a simplified approach to simulate drought induced mortality, the effect should be considered in future studies.

Strategies with the ORP in sand were more successful in terms of carbon assimilation compared to the strategies with the ORP in loam and clay. This can be explained with the higher transpiration rate of the ORP in sandy soil and therefore a higher carbon assimilation rate. This was also the case in a field study, where *Robinia pseudoacacia* showed higher transpiration rates grown in sandier soil, but also reacted more sensitive to meteorological conditions (Wu et al. 2015) and also align with the different transpiration in different soils in the model approach of Collins & Bras, 2007). However, although strategies in sand seem to be more successful, the efficiency of the least effective root profiles in sand were lower than the efficiency of the least effective profiles in loam and clay. This indicates that root profiles in sand should be better adapted to the environmental conditions. This might contribute to explaining the general trend for higher root-to-shoot ratios in coarser textured soils, as shown by Mokany et al. (2006), which may represent a strategy to compensate short-term environmental changes.

8.2 Optimal root profile and precipitation

In the last section the impact of different soil textures on the ORP's was discussed and the challenges of comparing the provided model output with observed root profiles were demonstrated. As shown in the last section, ORP's are adapted to the infiltration profile of the soil, which is not only determined by the soil texture but also by precipitation that infiltrates into the soil. The results of this study provide insights into how precipitation patterns affect ORP's. Reduced MAP by 20% leads, due to less water in the system, to lower transpiration rates and more drought stress indicated by a higher M_Ψ . Across all soil types, ORP's are shallower distributed under reduced MAP than the ORP's in the base scenario R_0 . Reduced MAP leads to a reduced infiltration rate into the soil. And as previously mentioned, roots compete with water loss through drainage and soil evaporation. With a lower infiltration rate, roots take up the infiltrated water before it can reach deeper soil layers resulting in a reduced infiltration depth. This is indicated by the maximum transpiration rate for shallower root profiles compared with the root profiles with the highest transpiration rates under the base MAP. Therefore, ORP's were deeper distributed under an increased MAP because more water was able to infiltrate deeper before the roots could absorb it.

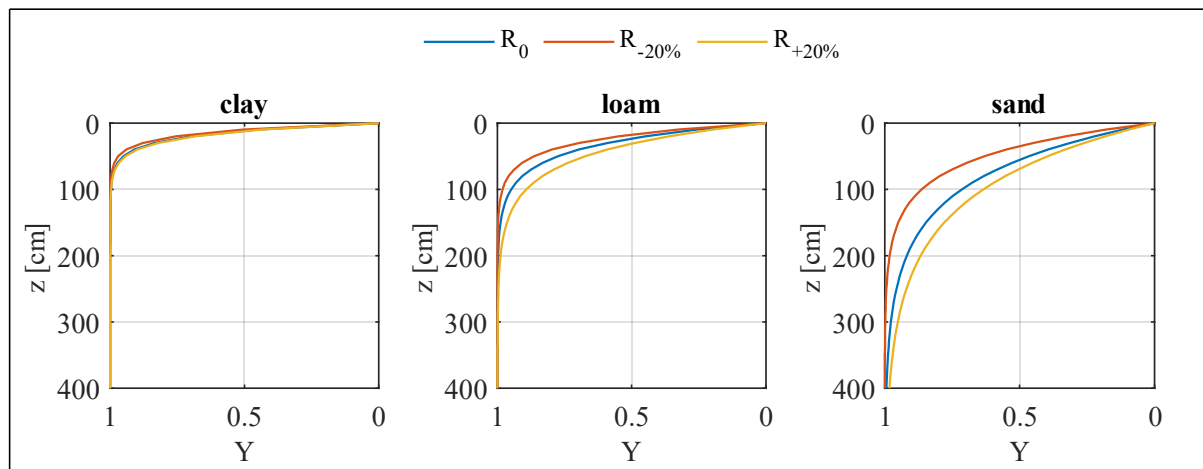


Figure 10 Optimal root profiles of the precipitation scenarios R_0 , $R_{-20\%}$ and $R_{+20\%}$; Cumulative root distribution as a function of β . Clay: $\beta=0.942$ (R_0), $\beta=0.932$ ($R_{-20\%}$), $\beta=0.944$ ($R_{+20\%}$); Loam: $\beta=0.971$ (R_0), $\beta=0.961$ ($R_{-20\%}$), $\beta=0.978$ ($R_{+20\%}$); Sand: $\beta=0.988$ (R_0), $\beta=0.980$ ($R_{-20\%}$), $\beta=0.990$ ($R_{+20\%}$).

The shift of the ORP's were in both directions the largest in sandy soil with 50% of BM_{root} in the first 34.0 cm, 57.4 cm, and 69.0 cm of the soil, from reduced to base to increased MAP. In loam, 50% of BM_{root} were located in the first 17.4 cm, 23.5 cm, and 31.2 cm, respectively. And in clay, 50% BM_{root} were located in the first 9.8 cm, 11.6 cm, and 12 cm of the soil column (Figure 10). Noteworthy is the minor effect to the ORP under increased MAP in clay. Due to the lower hydraulic conductivity, water movement in clay soil is less dynamic and the upmost soil layer tend to be fully saturated more often than in loam or sand and more rainwater is

therefore lost via runoff. This explains the lower effect of increased MAP in clay. The same principal leads to the largest effect in sandy soil, where water movement is more dynamic. In a study of Hertel et al. (2013) an increasing fine root production of *Fagus sylvatica* (L.) in the upper 30 cm of soil with decreasing MAP was observed. Since the roots in their study were only collected in the upper 30 cm information about the complete root profiles are missing. Still, this is here interpreted as an increase in fine root biomass in the upper soil, which aligns with the results of this study. Further, in the study of Hertel et al. (2013) the increase in fine root production was larger in sandy compared to more loamy soil. Which supports the different effect sizes in different soils of this study. However, interpreting increased fine root production in the upper soil is equivalent to an adaptation to a more shallower root profile can be seen as questionable; alternatively, it could be a general increase in root biomass without a change of the vertical fine root distribution. In contrast, another study focusing on the response of *Fagus sylvatica*'s root system across a precipitation gradient, where roots were also collected in deeper soil layers, no increase in total fine root biomass was observed with decreasing MAP (Meier et al. 2018).

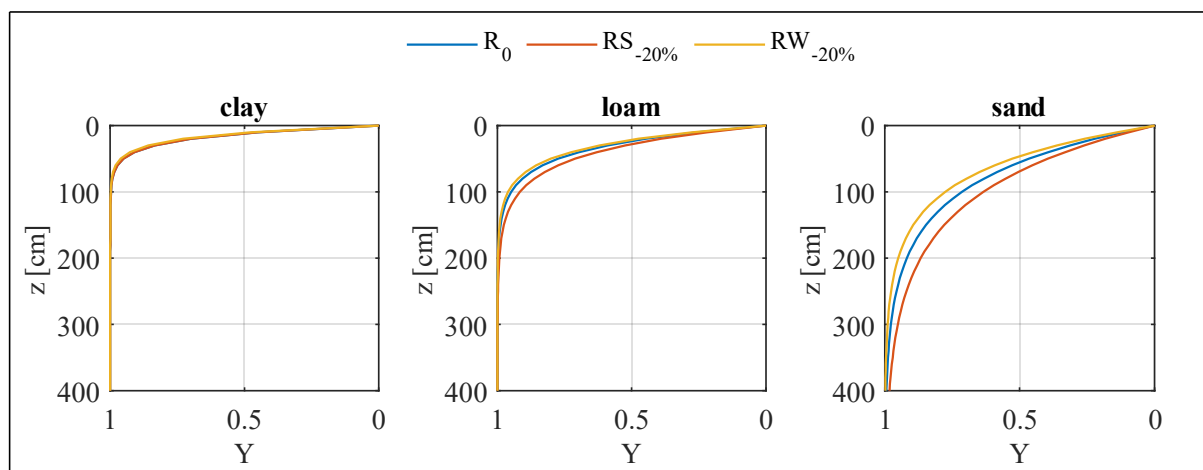


Figure 11 Optimal root profiles of the precipitation scenarios R_0 , $RS_{-20\%}$ and $RW_{-20\%}$; Cumulative root distribution as a function of β . Clay: $\beta=0.942$ (R_0), $\beta=0.942$ ($RS_{-20\%}$), $\beta=0.937$ ($RW_{-20\%}$); Loam: $\beta=0.971$ (R_0), $\beta=0.976$ ($RS_{-20\%}$), $\beta=0.968$ ($RW_{-20\%}$); Sand: $\beta=0.988$ (R_0), $\beta=0.990$ ($RS_{-20\%}$), $\beta=0.985$ ($RW_{-20\%}$).

Although, the study of Meier et al. (2018) also observed an increase of fine root biomass in the upper soil with decreasing MAP, but in contrast observed small coarse roots in deeper soil areas. In the model, only absorbing fine roots were considered and it was assumed that fine root distribution correlates with the coarser root system. This may be true for stable environmental conditions but could be misleading if soil water conditions are changing. Meier et al. (2018) stated, that it should be distinguished between short- and long-term plant responses to a reduced MAP. The development of deep roots to reach deeper water reservoirs is more pronounced in arid climates and could explain the weak correlation between MAP and rooting depth on a

global scale (Schenk and Jackson 2002). In summary, the provided pattern of the model could still be seen as plausible, as it describes local conditions which are supported by the findings of Meier et al. (2018) and Hertel et al. (2013). Further, it agrees with the hydraulic framework of Fan et al. (2017), where local rooting depth also correlates with MAP.

However, the results of this study also suggest that MAP alone is an insufficient parameter to identify the ORP, as the ORP's of the three scenarios (R_0 , $RS_{-20\%}$, $RW_{-20\%}$) with equal MAP differed (Figure 11). With reduced precipitation during the summer root profiles were deeper distributed in loam and sand, while equal in clay, compared to the R_0 precipitation. Again, the effect was the largest in the more dynamic sandy soil with 50% of BM_{root} in the first 68.9 cm of the soil (R_0 : 57.4 cm). In loam, 50% of BM_{root} were located in the first 28.5 cm of the soil (R_0 : 23.5 cm). In contrast, root profiles were shallower in all soil types under reduced winter precipitation, with 50% of BM_{root} in a depth of 10.6 cm in clay, 21.3 cm in loam and 45.9 cm in sand. This contrasting effect can be explained by the fact, that the roots were inactive and did not absorb water during the winter season, which allows the water to infiltrate deeper. While in summer, roots absorb the infiltrating water before it can reach the same depth. Although, strategies tested in clay showed lower transpiration rates and had more drought stress (M_Ψ) in the $RS_{-20\%}$ scenario, the ORP did not changed. This deviation of the expected model and the general shown pattern could be explained by increased runoff in winter. In the model, rainwater infiltrates in the first soil layer and is limited thereby by the maximum water content of this layer. The excess water is lost via runoff, no ponding or delayed infiltration was considered. The way infiltration was simplified appears to have limitations in that aspect.

However, the general pattern provided by the model is consistent with other models (Collins and Bras 2007; Rudd et al. 2014). And were plausible in relation to the results of Meier et al. (2018), where a reduced fine root biomass was observed in the first 30 cm of soil with decreasing precipitation in spring. Further, a study focusing on the water use of trees in Switzerland showed differences between Spruce, Beech, and Oaks in their ability to use water from winter precipitations, due to their adapted root systems to the hydraulic site conditions (Goldsmith et al. 2022). Underlining the made assumption and the presented results of this study, that root systems should be deeper distributed with decreasing summer precipitation and increasing winter precipitation.

8.3 Optimal root profile and temperature

Against the assumption that an increase in air temperature leads to an increased PET and therefore higher soil evaporation, no difference between the PET in the climate before (P_{79}) and

after (P_{00}) the year 2000 was provided by the model (Table 7). This may be explainable with the calculation of PET with the simplified form of the Penman-Monteith equation provided by Priestley and Taylor (1972). Which seems to show the smallest response to temperate change, compared with other approaches to calculate PET (McKenney and Rosenberg 1993).

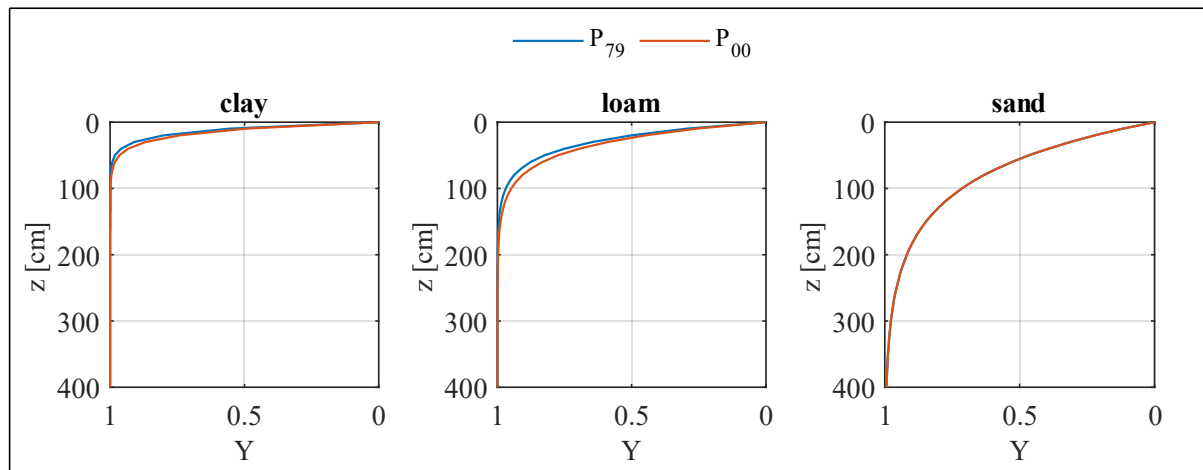


Figure 12 Optimal root profiles of the climate scenarios P_{79} and P_{00} ; Cumulative root distribution as a function of β . Clay: $\beta=0.922$ (P_{79}), $\beta=0.935$ (P_{00}); Loam: $\beta=0.966$ (P_{79}), $\beta=0.971$ (P_{00}); Sand: $\beta=0.988$ (P_{79}), $\beta=0.988$ (P_{00}).

However, ORP's were deeper distributed in clay and loam under the P_{00} climate compared with the ORP's under the P_{79} climate (Figure 12). In sandy soil, ORP's were equal distributed in these two climates. Further, across all soil types NPP was lower under the P_{00} climate. With regard to the results presented above, the effect of deeper distributed ORP's could be explained by the reduced summer precipitation after the year 2000. In summary, the model was not able to prove the hypothesis that an increase in temperature leads to deeper distributed root profiles. Since a correlation between rooting depth and annual PET was observed in temperate and boreal forests (Schenk and Jackson 2002), future studies should consider using a more accurate method to estimate PET.

8.4 Sensitivity analysis

In total 16 parameters were tested to identify the sensitivity of the provided ORP's to the parametrization of the model. It has to be mentioned that the settings of the sensitivity analysis with only 15 root profiles tested leads to a lower resolution in the output. However, if the parameters displayed no change in the ORP, their impact on the ORP can be considered as low. Only LAI and BM_{root} leaded in the settings of the sensitivity analysis to a shift of the ORP. A change in the LAI change the demand of transpiration and a change in BM_{root} leads to a change in the RWU capacity. Both parameters have therefore a comparable effect on the plant water status. An unbalanced ratio between these two plant traits, as it was tested in the sensitivity analysis by only changing one parameter, seem to have a major effect on M_{ψ} and leads therefore

to a change of the ORP's. The exceeded forest defoliation, as observed in the last decades in Europe were associated with more intense drought events in this time period (Senf et al. 2020). Those findings can be interpreted as a short-term adaptation to insufficient water supply by the root system to avoid cavitation damage (Wolfe et al. 2016). Indicating, that non optimal root profiles could be compensated by adapting the LAI. The dynamic response of trees to the environmental conditions and different allocation patterns of LAI and BM_{root} were not considered in this study but should be in further studies.

Although the other tested parameters had no impact on the ORP, some of them, such as specific root length, Ψ_{50} , $v_{\text{cmax}25}$ and the mortality rates M_b and M_Ψ had a large impact on the NPP. This seems to be unproblematic in the here presented model approach where water was considered as the only limiting factor and ORP's were determined based on the best carbon balance. In reality, tree growth depends also on other resources, such as N, P, and K (Schenk 2008). An implementation of these limitations in the model can reduce the carbon sequestration, as shown in the model approach of Goll et al. (2012). In this case, the mentioned parameters may have an impact on the ORP if a balance between carbon and other soil resources is required.

8.5 Model limitations

The here presented model is based on several assumptions and simplifications, leading to some limitations and uncertainties in the process of identifying the ORP.'s. These will be discussed in the next sections.

8.5.1 Hydraulic pathway

One of the main assumptions in the model was the assumption of steady-state transpiration ($RWU=T$), implying that trees had no water storage capacity. The implementation of the water storage capacity requires a more complex approach of RWU and Ψ_{leaf} and was therefore not considered in this study. The ability to compensate water loss through transpiration by using stored water in the plant tissues was observed to be crucial for maintaining carbon uptake and contribute to tree survival during droughts and can be seen as a key drought resistance trait (Preisler et al. 2022). Not taking water storage into account resulted in a potential overestimation of drought stress with the consequence of higher M_Ψ and lower carbon assimilation rates. The impact of the water storage capacity to the ORP stays unclear.

Further simplifications associated with the hydraulic pathway were the previously discussed approach of estimating PET and the rainwater infiltration in the first soil layer. The latter led to high runoff in clay soil and can explain the in general lower transpiration and NPP values of

strategies tested in clay. Both the simplified PET and infiltration approach have a direct effect on the soil moisture profile resulting in uncertainties of the ORP's, especially in finer textured soils. These approaches should be improved in future studies.

8.5.2 Plant physiological processes

In the model, stomata conductance was with the exception of light only limited by plant water status related factors, namely soil moisture content, VPD and Ψ_{leaf} . In the stomata model of Jarvis (1976), CO_2 and temperature were also considered. Because the model was designed to maximize carbon uptake while avoiding cavitation, it was assumed that there was no need to limit the stomata conductance due to CO_2 . Temperature, on the other hand, could be considered more important in the model, but only if the leaf temperature is used to limit stomata conductance. Since the leaf temperature was not calculated in the model due to uncertainties in the parametrization and a lack of data for evaluating the leaf temperature, it was also excluded from the approach for limiting the stomata aperture.

However, stomata conductance also impacts the leaf temperature, as transpiration has a cooling effect. To reduce the risk of overheating some species increase their stomata conductance during heatwaves, while other species were less sensitive (Marchin et al. 2022). Thermal damage was not included in the model, which may have an effect on the tree success. The tradeoff between risking thermal damage and increasing risk for cavitation could also lead, depending on the stomata strategy, to changes in the ORP.

Further, stomata strategies not only differ in their reaction to temperature but also in their response to water scarcity (Tardieu and Simonneau 1998). In the model, different stomata strategies were not considered. The stomata response in the model can be interpreted as an anisohydric stomata behavior as species operated with a low safety margin ($\Psi_{\text{leaf,min}}$ defined at 12% loss of conductivity) before cavitation becomes critical to maximize carbon uptake (Hartmann 2010). The implementation of different stomata behavior should be considered in future studies as the effect on the ORP could be significant.

8.5.3 Carbon balance

The biomass accumulation approach of the model is simplified and based on constant mortality and turnover rates based on educational guess. As a result, the values given for M_Ψ and NPP are not comparable with values from the literature. A more precise approach would require a comprehensive parameterization. However, within the model framework this approach is

sufficient to compare the success of strategies with different root profiles, as a change in the mortality rates M_b and M_Ψ showed no effect on the ORP in the sensitivity analysis.

8.6 Model evaluation

By considering the mentioned limitations and with respect to the discussed results, the dissimilarity between observed individual root profiles and the provided ORP's was evident. More congruent results could be achieved by parametrize the model to specific site conditions such as soil properties and plant characteristics (e.g., LAI and BM_{root}) and by adding additional tradeoffs such as nutrient availability and different stomata strategies. The general patterns provided by the model, showing different vertical fine root distributions across different soil types, align with observed root profiles in water-limited ecosystems determined by differently textured soils (Xu and Li 2008). The fine root patterns provided under reduced and increased MAP also align with observed fine root distributions across a precipitation gradient (Hertel et al. 2013; Meier et al. 2018). The changes of the ORP's with changes in the seasonality of precipitation were also supported by the literature (Meier et al. 2018; Goldsmith et al. 2022). Further, the model results are also in coincidence with global root studies, where the same patterns across environmental gradients were described (Schenk and Jackson 2002; Fan et al. 2017).

In summary, although the ORP's did not match with observed root profiles, the general pattern provided by the model showing different fine root distributions under different environmental conditions seem plausible with respect to the mentioned literature and under the assumption that water is the limiting factor.

8.7 Conclusion

The here presented study describes the hydrological conditions determining the vertical fine root distribution of trees. It gives insights into how root systems might alter under a changing climate. This was achieved by developing a process-based model that linked the hydraulic pathway from the soil through the plant to the atmosphere with the stomata aperture and other plant physiological processes such as photosynthesis, leaf water potential and the hydraulic conductivity of the plant. The model provides plausible patterns for vertical fine root distributions under the assumption that water is the limiting factor, as it is predicted for European forests as a consequence of climate change. If other limitations occur, such as nutrients, observed root profiles did not match with the model output. However, the results suggest that ORP's are progressively deeper distributed from fine to coarse textured soils. Changes in the mean annual precipitation resulted in shallower ORP's with decreased MAP

and in deeper ORP's with increased MAP. Seasonal changes in the precipitation while MAP was equal, led to deeper distributed ORP's with decreasing summer precipitation and to shallower distributed ORP's with decreasing winter precipitation. Due to a simplified approach to estimate PET and small temperature differences in the climate data, the effect of temperature on the ORP's remains unclear. Nonetheless, under the assumption that water is the limiting factor, ORP's are determined by the infiltration profile determined by soil texture, MAP, and seasonality of rainfall. These findings indicate that changes in the seasonality of precipitation and an increase of more intense drought events require an adaptation of root profiles. The findings therefore contribute to the knowledge of understanding forest diebacks in the past and may help to predict and prevent forest diebacks in the future.

9 Acknowledgements

I would like to thank the members of the “Ecological Modeling” working group for support and help during my project. Especially I want to thank my supervisors Prof. Dr. Philipp Porada and Dr. Christoph Reisdorff for critical and helpful feedback in questions about modeling and plant physiology. My thanks also go to my friends and family for their support and to ICDC, CEN, University of Hamburg for data support.

10 References

- Alani, A.M. and Lantini, L. 2020. Recent Advances in Tree Root Mapping and Assessment Using Non-destructive Testing Methods: A Focus on Ground Penetrating Radar. *Surveys in Geophysics* 41, pp. 605–646. doi: 10.1007/s10712-019-09548-6.
- Alduchov, O.A. and Eskridge, R.E. 1996. Improved Magnus Form Approximation of Saturation Vapor Pressure. *Journal of Applied Meteorology and Climatology* 35(4), pp. 601–609.
- Anderegg, W.R.L., Berry, J.A. and Field, C.B. 2012. Linking definitions, mechanisms, and modeling of drought-induced tree death. *Trends in plant science* 17(12), pp. 693–700. doi: 10.1016/j.tplants.2012.09.006.
- Bernacchi, C.J., Singaas, E.L., Pimentel, C., Portis, A.R. and Long, S.P. 2001. Improved temperature response functions for models of Rubisco-limited photosynthesis. *Global Change Biology* 21(3), pp. 253–259. doi: 10.1111/J.1365-3040.2001.00668.X.
- Bhaskar, R. and Ackerly, D.D. 2006. Ecological relevance of minimum seasonal water potentials. *Physiologia Plantarum* 127(3), pp. 353–359. doi: 10.1111/j.1399-3054.2006.00718.x.
- Bonan, G. 2019a. Leaf Photosynthesis. In: *Climate Change and Terrestrial Ecosystem Modeling*. Cambridge University Press, pp. 167–188. doi: 10.1017/9781107339217.012.
- Bonan, G. 2019b. Plant Hydraulics. In: *Climate Change and Terrestrial Ecosystem Modeling*. Cambridge University Press, pp. 213–227. doi: 10.1017/9781107339217.014.
- Bonan, G. 2019c. Soil Moisture. In: *Climate Change and Terrestrial Ecosystem Modeling*. Cambridge University Press, pp. 115–133. doi: 10.1017/9781107339217.009.
- Bonan, G. 2019d. Vegetation Demography. In: *Climate Change and Terrestrial Ecosystem Modeling*. Cambridge University Press, pp. 344–364. doi: 10.1017/9781107339217.020.
- Carsel, R.F. and Parrish, R.S. 1988. Developing Joint Probability Distributions of Soil Water Retention Characteristics. *Water Resources Research* 24(5), pp. 755–769.
- Češljarić, G. et al. 2022. Impact of an Extremely Dry Period on Tree Defoliation and Tree Mortality in Serbia. *Plants* 11(10), pp. 1–17. doi: 10.3390/plants11101286.
- Chang, R., Fu, B., Liu, G., Yao, X. and Wang, S. 2012. Effects of soil physicochemical properties and stand age on fine root biomass and vertical distribution of plantation forests

- in the Loess Plateau of China. *Ecological Research* 27(4), pp. 827–836. doi: 10.1007/s11284-012-0958-0.
- Chapin, F.S.I. and Eviner, V.T. 2007. Biogeochemistry of Terrestrial Net Primary Production. In: *Treatise on Geochemistry*. pp. 1–35. doi: 10.1016/B0-08-043751-6/08130-5.
- Collins, D.B.G. and Bras, R.L. 2007. Plant rooting strategies in water-limited ecosystems. *Water Resources Research* 43(6), pp. 1–10. doi: 10.1029/2006WR005541.
- Eissenstat, D.M., Wells, C.E., Yanai, R.D. and Whitbeck, J.L. 2000. Building roots in a changing environment: Implications for root longevity. *New Phytologist* 147(1), pp. 33–42. doi: 10.1046/j.1469-8137.2000.00686.x.
- Fan, Y., Miguez-Macho, G., Jobbágy, E.G., Jackson, R.B. and Otero-Casal, C. 2017. Hydrologic regulation of plant rooting depth. *Proceedings of the National Academy of Sciences* 114(40), pp. 10572–10577. doi: 10.1073/pnas.1712381114.
- Farquhar, G.D., Caemmerer, S. and Berry, J.A. 1980. A biochemical model of photosynthetic CO₂ assimilation in leaves of C₃ species. *Planta* 149(1), pp. 78–90.
- Farquhar, G.D. and Sharkey, T.D. 1982. Stomatal conductance and photosynthesis. *Annual Review of Plant Physiology* 33, pp. 317–345.
- Finér, L. et al. 2007. Variation in fine root biomass of three European tree species: Beech (*Fagus sylvatica* L.), Norway spruce (*Picea abies* L. Karst.), and Scots pine (*Pinus sylvestris* L.). *Plant Biosystems* 141(3), pp. 394–405. doi: 10.1080/11263500701625897.
- Gale, M.R. and Grigal, D.F. 1987. Vertical root distribution of northern tree species in relation to successional status. *Canadian Journal of Forest Research* 17, pp. 829–834. doi: 10.1139/x87-131.
- van Genuchten, M.Th. 1980. A closed-form equation for predicting the hydraulic conductivity of unsaturated soils. *Soil Science Society of America Journal* 44(5), pp. 892–898. doi: 10.2136/sssaj1980.03615995004400050002x.
- Goldsmith, G.R., Allen, S.T., Braun, S., Siegwolf, R.T.W. and Kirchner, James W. 2022. Climatic influences on summer use of winter precipitation by trees. *Geophysical Research Letters* 49. doi: 10.1029/2022GL098323.
- Goll, D.S. et al. 2012. Nutrient limitation reduces land carbon uptake in simulations with a model of combined carbon, nitrogen and phosphorus cycling. *Biogeosciences* 9(9), pp. 3547–3569. doi: 10.5194/bg-9-3547-2012.

- Grillakis, M.G. 2019. Increase in severe and extreme soil moisture droughts for Europe under climate change. *Science of the Total Environment* 660, pp. 1245–1255. doi: 10.1016/j.scitotenv.2019.01.001.
- Hartmann, H. 2010. Will a 385 million year-struggle for light become a struggle for water and for carbon? - How trees may cope with more frequent climate change-type drought events. *Global Change Biology* 17(1), pp. 642–655. doi: 10.1111/j.1365-2486.2010.02248.x.
- Hartmann, H. et al. 2018. Research frontiers for improving our understanding of drought-induced tree and forest mortality. *New Phytologist* 218(1), pp. 15–28. doi: 10.1111/nph.15048.
- Hartmann, H., Bahn, M., Carbone, M. and Richardson, A.D. 2020. Plant carbon allocation in a changing world – challenges and progress: introduction to a Virtual Issue on carbon allocation. *New Phytologist* 227, pp. 981–988. doi: <https://doi.org/10.1111/nph.16757>.
- He, L., Chen, J.M., Pan, Y., Birdsey, R. and Kattge, J. 2012. Relationships between net primary productivity and forest stand age in U.S. forests. *Global Biogeochemical Cycles* 26(3). doi: 10.1029/2010GB003942.
- Hersbach, H. et al. 2020. The ERA5 global reanalysis. *Quarterly Journal of the Royal Meteorological Society* 146(730), pp. 1999–2049. doi: 10.1002/qj.3803.
- Hertel, D., Strecker, T., Müller-Haubold, H. and Leuschner, C. 2013. Fine root biomass and dynamics in beech forests across a precipitation gradient - Is optimal resource partitioning theory applicable to water-limited mature trees? *Journal of Ecology* 101(5), pp. 1183–1200. doi: 10.1111/1365-2745.12124.
- Ho, M.D., Rosas, J.C., Brown, K.M. and Lynch, J.P. 2005. Root architectural tradeoffs for water and phosphorus acquisition. *Functional Plant Biology* 32(8), pp. 737–748. doi: 10.1071/FP05043.
- Hodge, A., Berta, G., Doussan, C., Merchan, F. and Crespi, M. 2009. Plant root growth, architecture and function. *Plant and Soil* 321(1–2), pp. 153–187. doi: 10.1007/s11104-009-9929-9.
- Huang, X., Shi, Z.H., Zhu, H.D., Zhang, H.Y., Ai, L. and Yin, W. 2016. Soil moisture dynamics within soil profiles and associated environmental controls. *Catena* 136, pp. 189–196. doi: 10.1016/j.catena.2015.01.014.

- IPCC. 2022. IPCC, 2022: Climate Change 2022: Impacts, Adaptation, and Vulnerability. In: Pörtner, H.-O. et al. eds. *Contribution of Working Group II to the Sixth Assessment Report of the Intergovernmental Panel on Climate Change*. Cambridge, UK and New York, NY, USA: Cambridge University Press, pp. 3056–pp. doi: 10.1017/9781009325844.
- Jackson, R.B., Canadell, J., Ehleringer, J.R., Mooney, H.A., Sala, O.E. and Schulze, E.D. 1996. A global analysis of root distributions for terrestrial biomes. *Oecologia* 108(3), pp. 389–411. doi: 10.1007/BF00333714.
- Jacobsen, A.L., Ewers, F.W., Pratt, R.B., Iii, W.A.P. and Davis, S.D. 2005. Do Xylem Fibers Affect Vessel Cavitation Resistance? *Plant physiology* 139(1), pp. 546–556. doi: 10.1104/pp.104.058404.
- Jarvis, P.G. 1976. The interpretation of the variations in leaf water potential and stomatal conductance found in canopies in the field. *Philosophical Transactions of the Royal Society of London. B, Biological Sciences* 273(927), pp. 593–610. doi: 10.1098/rstb.1976.0035.
- Jobbágy, E.G. and Jackson, R.B. 2001. The distribution of soil nutrients with depth: Global patterns and the imprint of plants. *Biogeochemistry* 53, pp. 51–77.
- Li, S., Feifel, M., Karimi, Z., Schuldt, B., Choat, B. and Jansen, S. 2015. Leaf gas exchange performance and the lethal water potential of five European species during drought. *Tree Physiology* 36(2), pp. 179–192. doi: 10.1093/treephys/tpv117.
- Majdi, H. 1996. Root sampling methods-applications and limitations of the minirhizotron technique. *Plant and Soil* 185, pp. 255–258.
- Marchin, R.M., Backes, D., Ossola, A., Leishman, M.R., Tjoelker, M.G. and Ellsworth, D.S. 2022. Extreme heat increases stomatal conductance and drought-induced mortality risk in vulnerable plant species. *Global Change Biology* 28(3), pp. 1133–1146. doi: 10.1111/gcb.15976.
- McDowell, N. et al. 2008. Mechanisms of plant survival and mortality during drought: Why do some plants survive while others succumb to drought? *New Phytologist* 178(4), pp. 719–739. doi: 10.1111/j.1469-8137.2008.02436.x.
- McKenney, M.S. and Rosenberg, N.J. 1993. Sensitivity of some potential evapotranspiration estimation methods to climate change. *Agricultural and Forest Meteorology* 64(1–2), pp. 81–110. doi: 10.1016/0168-1923(93)90095-Y.

- Meier, I.C. et al. 2018. The Deep Root System of *Fagus sylvatica* on Sandy Soil: Structure and Variation Across a Precipitation Gradient. *Ecosystems* 21(2), pp. 280–296. doi: 10.1007/s10021-017-0148-6.
- Mokany, K., Raison, R.J. and Prokushkin, A.S. 2006. Critical analysis of root: Shoot ratios in terrestrial biomes. *Global Change Biology* 12(1), pp. 84–96. doi: 10.1111/j.1365-2486.2005.001043.x.
- Norddeutscher Klimamonitor. 2023. *Norddeutschland: Vegetationsperiode (1986-2015)*. Available at: <https://www.norddeutscher-klimamonitor.de/klima/1986-2015/jahr/vegetationsperiode/norddeutschland/coastdat-1.html> [Accessed: 13 November 2023].
- Obladen, N. et al. 2021. Tree mortality of European beech and Norway spruce induced by 2018-2019 hot droughts in central Germany. *Agricultural and Forest Meteorology* 307. doi: 10.1016/j.agrformet.2021.108482.
- Ooeda, H., Terashima, I. and Taneda, H. 2017. Intra-specific trends of lumen and wall resistivities of vessels within the stem xylem vary among three woody plants. *Tree Physiology* 38(2), pp. 223–231. doi: 10.1093/treephys/tpx114.
- Ostonen, I. et al. 2007. Specific root length as an indicator of environmental change. *Plant Biosystems* 141(3), pp. 426–442. doi: 10.1080/11263500701626069.
- Pammenter, N.W. and Willigen, C. Vander. 1998. A mathematical and statistical analysis of the curves illustrating vulnerability of xylem to cavitation. In: *Tree Physiology*. Oxford University Press, pp. 589–593. doi: 10.1093/treephys/18.8-9.589.
- Pierret, A., Maeght, J.L., Clément, C., Montoroi, J.P., Hartmann, C. and Gonkhamdee, S. 2016. Understanding deep roots and their functions in ecosystems: An advocacy for more unconventional research. *Annals of Botany* 118(4), pp. 621–635. doi: 10.1093/aob/mcw130.
- Preisler, Y. et al. 2022. The importance of tree internal water storage under drought conditions. *Tree Physiology* 42(4), pp. 771–783. doi: 10.1093/treephys/tpab144.
- Priestley, C.H.B. and Taylor, R.J. 1972. On the Assessment of Surface Heat Flux and Evaporation Using Large-Scale Parameters. *Monthly Weather Review* 100(2), pp. 81–92. doi: 10.1175/1520-0493(1972)100<0081:OTAOSH>2.3.CO;2.

- Qi, Y. et al. 2022. Applicability of stomatal conductance models comparison for persistent water stress processes of spring maize in water resources limited environmental zone. *Agricultural Water Management* 277(2023). doi: 10.1016/j.agwat.2022.108090.
- Richards, L.A. 1931. Capillary conduction of liquids through porous mediums. *Journal of Applied Physics* 1(5), pp. 318–333. doi: 10.1063/1.1745010.
- Ristic, Z. and Jenks, M.A. 2002. Leaf cuticle and water loss in maize lines differing in dehydration avoidance. *Journal of Plant Physiology* 159(6), pp. 645–651. doi: 10.1078/0176-1617-0743.
- Ritchie, J.T. 1972. Model for predicting evaporation from a row crop with incomplete cover. *Water Resources Research* 8(5), pp. 1204–1213. doi: 10.1029/WR008i005p01204.
- Rose, D.A. 1996. The dynamics of soil water following single surface wettings. *European Journal of Soil Science* 47(1), pp. 21–31. doi: 10.1111/j.1365-2389.1996.tb01368.x.
- Rudd, K., Albertson, J.D. and Ferrari, S. 2014. Optimal root profiles in water-limited ecosystems. *Advances in Water Resources* 71, pp. 16–22. doi: 10.1016/j.advwatres.2014.04.021.
- Schenk, H.J. 2008. The Shallowest Possible Water Extraction Profile: A Null Model for Global Root Distributions. *Vadose Zone Journal* 7(3), pp. 1119–1124. doi: 10.2136/vzj2007.0119.
- Schenk, H.J. and Jackson, R.B. 2002. The global biogeography of roots. *Ecological Monographs* 72(3), pp. 311–328. doi: 10.1890/0012-9615(2002)072[0311:TGBOR]2.0.CO;2.
- Scholz, A., Rabaey, D., Stein, A., Cochard, H., Smets, E. and Jansen, S. 2013. The evolution and function of vessel and pit characters with respect to cavitation resistance across 10 *Prunus* species. *Tree Physiology* 33(7), pp. 684–694. doi: 10.1093/treephys/tpt050.
- Seneviratne, S.I. et al. 2010. Investigating soil moisture-climate interactions in a changing climate: A review. *Earth-Science Reviews* 99(3–4), pp. 125–161. doi: 10.1016/j.earscirev.2010.02.004.
- Senf, C., Buras, A., Zang, C.S., Rammig, A. and Seidl, R. 2020. Excess forest mortality is consistently linked to drought across Europe. *Nature Communications* 11(1), pp. 1–8. Available at: <http://dx.doi.org/10.1038/s41467-020-19924-1>.

- Tardieu, F. and Simonneau, T. 1998. Variability among species of stomatal control under fluctuating soil water status and evaporative demand: modelling isohydric and anisohydric behaviours. *Journal of Experimental Botany* 49, pp. 419–432.
- Teuling, A.J. 2018. A hot future for European droughts. *Nature Climate Change* 8(5), pp. 364–365. doi: 10.1038/s41558-018-0154-5.
- Thomas, F.M. 2000. Vertical rooting patterns of mature *Quercus* trees growing in different soil types in northern Germany. *Plant Ecology* 147, pp. 95–103. doi: 10.1023/A:1009841921261.
- Tjoelker, M.G., Oleksyn, J., Lorenc-Plucinska, G. and Reich, P.B. 2009. Acclimation of respiratory temperature responses in northern and southern populations of *Pinus banksiana*. *New Phytologist* 181(1), pp. 218–229. doi: 10.1111/j.1469-8137.2008.02624.x.
- Tyree, M.T. 2003. Hydraulic limits on tree performance: Transpiration, carbon gain and growth of trees. *Trees - Structure and Function* 17(2), pp. 95–100. doi: 10.1007/s00468-002-0227-x.
- Tyree, M.T., Davis, S.D. and Cochard, H. 1994. Biophysical perspectives of Xylem evolution: Is there a tradeoff of hydraulic efficiency for vulnerability to dysfunction? *IWA Journal* 15(4), pp. 335–360.
- Tyree, M.T. and Zimmermann, M.H. 2002. Failure and “Senescence” of Xylem Function. *Xylem Structure and the Ascent of Sap* 2, pp. 229–237. doi: 10.1007/978-3-662-04931-0_8.
- Wolfe, B.T., Sperry, J.S. and Kursar, T.A. 2016. Does leaf shedding protect stems from cavitation during seasonal droughts? A test of the hydraulic fuse hypothesis. *New Phytologist* 212, pp. 1007–1018. doi: 10.1111/nph.14087.
- Wu, Y.Z., Huang, M. Bin and Warrington, D.N. 2015. Black Locust Transpiration Responses to Soil Water Availability as Affected by Meteorological Factors and Soil Texture. *Pedosphere* 25(1), pp. 57–71. doi: 10.1016/S1002-0160(14)60076-X.
- Xu, G.Q. and Li, Y. 2008. Rooting depth and leaf hydraulic conductance in the xeric tree *Haloxylon ammodendron* growing at sites of contrasting soil texture. *Functional Plant Biology* 35(12), pp. 1234–1242. doi: 10.1071/FP08175.

11 Appendix

11.1 Model description

11.1.1 Hydraulic pathway

Soil water content

In the model, a soil column with a depth of 5 m, separated into uniform soil layers with a thickness of 0.1 m each, was implemented. Rainfall infiltrates in the upmost soil layer and was limited by the difference between maximum water storage capacity ($W_{max,i}$) and actual water content of the soil layer (W_i). Due to this restriction, water that could not infiltrate the soil was lost as runoff. The model did not account for ponding or canopy interception.

Water movement between adjusted soil layers was then described by a general derivation of the finite difference approximation for the Richard Equation (Eq. 2 & 3)(Richards 1931; Bonan 2019c):

$$Q_i = -\frac{K_{soil,i+1/2}}{\Delta z_{i+1/2}}(\Psi_{soil,i} - \Psi_{soil,i+1}) - K_{soil,i+1/2} \quad (3)$$

$$Q_{i-1} = -\frac{K_{soil,i-1/2}}{\Delta z_{i-1/2}}(\Psi_{soil,i-1} - \Psi_{soil,i}) - K_{soil,i-1/2} \quad (4)$$

where Q_i and Q_{i-1} are the water fluxes in, respectively out of the soil layer, $K_{soil,i\pm 1/2}$ is the arithmetic mean of soil hydraulic conductivity ($K_{soil,i}$) of adjusted soil layers. $\Delta z_{i\pm 1/2}$ is the distance between adjusted soil layers and $\Psi_{soil,i}$ the hydraulic head of the soil layer combining matric potential and gravitational potential ($\Psi_{soil,i} + z_i$), with $z=0$ at the surface and $z<0$ in the downward direction. Matric potential and hydraulic conductivity depend on the saturation (θ) of the soil layer, and are described by the van Genuchten model (van Genuchten 1980):

$$S_{e,i} = \frac{\theta_i - \theta_{res,i}}{\theta_{sat,i} - \theta_{res,i}} = \left[1 + (vG_\alpha |\Psi_{soil,i}|)^{vG_n} \right]^{-vG_m} \quad (5)$$

$$K_i = K_{sat} \sqrt{S_{e,i}} \left[1 - (1 - vG_m \sqrt{S_{e,i}})^{vG_m} \right]^2 \quad (6)$$

where $S_{e,i}$ is the effective saturation, with θ_i the actual, $\theta_{sat,i}$ the maximum and $\theta_{res,i}$ the residual volumetric water content of soil layer i . vG_n is the pore-size distribution index, with $vG_m = 1 - 1/vG_n$, vG_α the inverse of the air entry potential, and K_{sat} the hydraulic conductivity at saturation, these parameters were obtained from the work of (Carsel and Parrish 1988).

Volumetric water content θ is defined as depth of water per unit depth of soil. Water content per soil layer is written as $W_i = \theta_i \Delta z$, with Δz the soil layer thickness. Changes in the water content for the next time step is then:

$$\frac{W_{i,t+1}}{dt} = \frac{W_{i,t}}{dt} + Q_i + Q_{i-1} - RWU_i \quad (7)$$

where RWU_i is soil layer specific RWU (Eq. 14). In the upmost soil layer, soil evaporation (E), a fraction of PET , occurs as an additional sink term (Eq. 8 & 9).

$$PE = PET - PT \quad (8)$$

where PE is potential evaporation and PT potential transpiration. Actual soil evaporation is then:

$$E = PE * S_{e,1} \quad (9)$$

PT can be described as a fraction of PET depending on LAI (Ritchie 1972):

$$PT = PET * (1 - e^{(-\sigma * LAI)}) \quad (10)$$

where $\sigma = 0.4$, as used in the work of Collins and Bras (2007).

Potential evapotranspiration is calculated with a simplification of the Penman-Richard Equation developed by Priestley and Taylor (1972) based on radiation:

$$\lambda PET = \frac{\Delta}{\Delta + \gamma} (R_n - G) * \frac{\alpha}{\rho_w} \quad (11)$$

where λ is the latent heat of evaporation of water, $\Delta = de_s/dt_{air}$ is here the derivate of saturated vapor pressure with respect to t_{air} , α is in this context the Priestley-Taylor parameter; a corrector factor in this study set to 1.3. γ is the psychrometric constant which describes the relationship between air temperature and humidity. G is the ground heat flux and R_n is the net radiation, written as:

$$R_n = s_{rad}(1 - \alpha_R) + \varepsilon_R l_{rad} - \varepsilon_R \sigma_R t_{surf}^4 \quad (12)$$

Where s_{rad} and l_{rad} is short- and longwave radiation, respectively. σ_R is the Boltzmann constant α_R is the albedo, ε_R the emissivity and t_{surf} the temperature of the soil surface. t_{surf} is obtained from Porada (not in press).

Transpiration and root water uptake

In the model, steady-state transpiration was assumed and no water storage in the plant was considered, so that:

$$T = RWU \quad (13)$$

Transpiration is described as a diffusive process where g_{sw} is stomatal conductance and VPD divided by ambient air pressure (P_{air}) which is defined as the atmospheric demand (Bonan 2019b):

$$T = g_{sw} * \frac{VPD}{P_{air}} * LAI \quad (14)$$

and is limited by potential transpiration:

$$T = \min\{T, PT\} \quad (15)$$

VPD is the gradient between vapor pressure at saturation and actual vapor pressure, written as:

$$VPD = e_s - e_s r_{hu} \quad (16)$$

With saturation vapor pressure described with a Magnus form equation (Alduchov and Eskridge 1996):

$$e_s = 0.61094 e^{\frac{17.625 t_{air}}{t_{air} + 243.05}} \quad (17)$$

here, t_{air} in Kelvin.

In the model, PT is assumed to be the main driver for transpiration, but not a limiting factor for stomata conductance. These terms define water loss through transpiration, while allowing trees to keep their stomata open, maximizing CO_2 diffusion into the leaves even under low PT conditions, if not limited by other factors (see below).

However, transpiration was then fractioned into RWU_i with respect to β_{wet} , a soil wetness factor and Y_{frac} (Bonan 2019c):

$$\beta_{wet,i} = \begin{cases} \frac{\Psi_{soil,i} - \Psi_{WP}}{\Psi_{opt} - \Psi_{WP}} & \Psi_{soil,i} > \Psi_{WP} \\ 0 & \Psi_{soil,i} \leq \Psi_{WP} \end{cases} \quad (18)$$

$$RWU_i = T \left(\frac{\beta_{wet,i} Y_{frac,i}}{\sum_{i=1}^N \beta_{wet,i} Y_{frac,i}} \right) \quad (19)$$

where Ψ_{WP} is the wilting point and Ψ_{opt} is the soil water potential at $\beta_{wet}=1$. The factor β_{wet} enables trees to compensate for dry soil layers by giving more weight to RWU_i in wetter layers. RWU_i is limited by a maximum root water uptake capacity ($RWU_{max,i}$) which can be described by Darcy's Law $Q=K\Delta\Psi$, with K the conductance of the pathway and $\Delta\Psi$, the water potential gradient, for $RWU_{max,i}$ written as (Bonan, 2019a):

$$RWU_{max,i} = K_{root,i} (\Psi_{soil,i} - \Psi_{leaf,min}) \quad (20)$$

$$RWU_{max,i} = \min \left\{ RWU_{max,i}, \frac{W_i - W_{WP}}{dt} \right\} \quad (21)$$

where $K_{root,i}$ is the soil layer specific soil to stem conductance, $\Psi_{leaf,min}$ is the minimum leaf water potential before the risk of embolism becomes critical and W_{WP} is the water content at wilting point. If RWU_i was limited by Equation 16, total RWU would be smaller than T . To align with the steady-state assumption, g_{sw} was manually reduced.

Plant conductance

The total plant conductance (K_{plant}) of the soil-to-leaf pathway can be defined as the inverse of in series connected belowground (R_b) and aboveground (R_a) plant hydraulic resistances, following Ohm's Law K_{plant} can be written as (Bonan 2019b):

$$K_{plant} = \frac{1}{(R_b + R_a)} (1 - PLC) \quad (22)$$

K_{plant} is here reduced by the potential loss of conductivity (PLC) which in turn depends on Ψ_{leaf} (see below). Aboveground resistance is thereby described as:

$$R_a = \frac{1}{K_a * LAI} \quad (23)$$

where K_a is the aboveground conductance of the stem-to-leaf pathway per LAI , in the model defined as constant. The total belowground resistance R_b is composed of parallel connected soil layer specific resistances of the in series connected soil-to-root and root-to-stem pathway. Here expressed as $K_{root,i}$ with $K_{s,i}$ the soil-to-root conductance, and $K_{r,i}$ the root-to-stem conductance per soil layer respectively, written as (Figure 2) (Bonan 2019b):

$$R_b = \left(\sum_{i=1}^N K_{root,i} \right)^{-1} \quad (24)$$

with:

$$K_{root,i} = \frac{1}{\frac{1}{K_{s,i}} + \frac{1}{K_{r,i}}} \quad (25)$$

Root-to-stem conductance per soil layer is written as:

$$K_{r,i} = \frac{BM_{root} Y_{frac,i}}{R_r^*} \quad (26)$$

where R_r^* is the root resistivity which defines the hydraulic resistance per root mass. Soil-to-root conductance depends on the fine root distribution in the soil layer and the soil conductivity K_{soil} , which depends on the soil water content. In the model, fine roots are assumed to be evenly distributed in each soil layer and $K_{s,i}$ is then described as:

$$K_{s,i} = \frac{2\pi L_{r,i} K_{soil,i}}{\ln(r_{s,i}/r_r)} \quad (27)$$

$L_{r,i}$ thereby stands for the root length per soil layer, depending on specific root length r_l , total fine root biomass BM_{root} and the root distribution Y_{frac} :

$$L_{r,i} = r_l (BM_{root} * Y_{frac,i}) \quad (28)$$

$$r_l = \frac{1}{\rho_r \pi r_r^2} \quad (29)$$

where r_r is the mean fine root radius, ρ_r is the root tissue density, and $r_{s,i}$ is the radius of the soil cylinder occupied by the root. With roots distributed uniformly, the root length density can be described as the inverse of the soil volume associated with a unit length of root and can be transformed to $r_{s,i}$ (Bonan 2019b):

$$r_{s,i} = \frac{1}{\sqrt{\pi L_{r,i}}} \quad (30)$$

In this context, $r_{s,i}$ represents half of the distance between uniformly distributed fine roots.

11.1.2 Plant physiological processes

Leaf water potential

For calculation Ψ_{leaf} total RWU can also be written, by applying Darcy's Law as (Bonan 2019b):

$$RWU = K_{plant} (\Psi_{soil} - \rho_w g h - \Psi_{leaf}) \quad (31)$$

where the term $\rho_w g h$ describes the gravitational potential, where ρ_w is the density of water, g the gravitational acceleration and h tree height. Ψ_{soil} represents the soil water potential which depends on water content in the soil and varies across different soil layers. Aboveground biomass is connected by their root system with several soil layers. Therefore, a single value for $\Psi_{soil,i}$ is necessary. In respect to different root profiles Ψ_{soil} is calculated with $RWU_{max,i}$ as a weighted mean, so that (Bonan 2019b):

$$\Psi_{soil} = \sum_{i=1}^N \Psi_{soil,i} \frac{RWU_{max,i}}{\sum RWU_{max,i}} \quad (32)$$

by substituting Eq. 17 into Eq. 10 and rearranging for Ψ_{leaf} . It can be described under steady-state transpiration as follows (Bonan 2019b):

$$\Psi_{leaf} = \Psi_{soil} - \rho_w g h - \frac{T}{K_{plant}} \quad (33)$$

Thereby, Ψ_{leaf} was limited to -6 MPa to avoid extreme values during severe drought events. Ψ_{leaf} is an indicator of the plant's water status, mainly determined by soil water availability and

transpiration (Bhaskar and Ackerly 2006). Ψ_{leaf} decreases when transpiration increases and/or soil water availability decreases. Water-stressed trees can exhibit low values of Ψ_{leaf} which increase the risk for cavitation (McDowell et al. 2008). The vulnerability to drought induced embolism and the percentage of conductivity loss (PLC) can be described by a vulnerability-curve (Pammenter and Willigen 1998):

$$PLC = \frac{100}{1 + \exp\left[\frac{\alpha}{25}(\Psi_{leaf} - \Psi_{50})\right]} \quad (34)$$

where α is a slope parameter, and Ψ_{50} indicates the point at which Ψ_{leaf} results in a 50% loss of conductivity. In the model, $\Psi_{leaf,min}$ was defined at 12% loss of conductivity.

Stomata conductance

Stomata conductance (g_{sw}) is represented by an adaption of the empirical multiplicative model, introduced by Jarvis (1976). In the model, the multiplicative approach is changed to a minimum approach, to avoid interactions of multiple factors restricting g_{sw} . The following limitation factors taken over from Jarvis (1976) were used: VPD , Ψ_{leaf} , and light (here downwelling shortwave radiation s_{rad}), while air temperature and ambient CO_2 were not considered as limiting factors for g_{sw} . However, soil water content (θ) was implemented as an additional limiting factor (Qi et al. 2022). Hence g_{sw} was described as:

$$g_{sw} = \min\{f(s_{rad}), f(VPD), f(\Psi_{leaf}), f(\theta)\} \quad (35)$$

with

$$f(s_{rad}) = g_0 + g_{max} g_1 \left(s_{rad} - \frac{g_0}{g_{max}}\right) \left(g_{max} + g_1 \left(s_{rad} - \frac{g_0}{g_{max}}\right)\right) \quad (36)$$

$$f(VPD) = g_0 + g_{max}(1 - g_2 VPD) \quad (37)$$

$$f(\Psi_{leaf}) = g_0 + g_{max}(1 - e^{-g_3(\Psi_{leaf} - \Psi_{leaf,min})}) \quad (38)$$

where g_1 , g_2 and g_3 are slope parameters.

$$f(\theta) = g_0 + g_{max} \frac{(\theta - \theta_{WP})}{(\theta_{fc} - \theta_{WP})} \quad (39)$$

In this context, θ represents the mean of θ_i , weighted in the same manner as Ψ_{soil} for Ψ_{leaf} (Eq. 18). θ_{fc} is soil water content at field capacity, in the model defined as 50% of θ_{sat} . θ_{WP} is the soil water content at wilting point. All terms are limited by a minimum conductance g_0 and a maximum conductance g_{max} .

In respect to the different molecule sizes of water and CO₂, stomatal conductance for CO₂ (g_{lc}) is smaller compared to g_{sw} . With the assumption that leaf boundary conductance (g_{bw}) follows $g_{bw} \gg g_{sw}$, leaf boundary conductance can be ignored and g_{lc} is then described as (Bonan 2019a):

$$g_{lc} = \frac{g_{sw}}{1.6} \quad (40)$$

with g_{lc} , the diffusive supply of ambient CO₂ into the leaf was substituted into the photosynthesis model (see below) to solve for the intercellular CO₂ concentration (Bonan 2019a).

Photosynthesis

The process of carbon assimilation was simulated with the photosynthesis model for C3 species from Farquhar, von Caemmerer and Berry (FvCB model) (Farquhar et al. 1980). In the FvCB model, total CO₂ assimilation (A_{total}) is limited by two terms, first the rubisco-limited rate (A_C), and second, the light limited rate (A_J). Total Assimilation is then:

$$A_{total} = \min\{A_C, A_J\} - R_d \quad (41)$$

$$A_C = \frac{v_{c,max}(c_i - \Gamma)}{c_i + K_C \left(1.0 + \left(\frac{O_2}{K_O}\right)\right)} \quad (42)$$

$$A_J = \frac{J(c_i - \Gamma)}{4.5c_i + 1.5\Gamma} \quad (43)$$

where $v_{c,max}$ represents the maximum rate of carboxylation, Γ is the carbon compensation point, O_2 the atmospheric O₂ concentration, and K_C and K_O are the Michael-Menten constants for carbon and oxygen, respectively.

R_d is the leaf respiration and depends on temperature, following a standard Q10 relationship (Tjoelker et al. 2009):

$$R_d = R_{d0} Q_{10}^{(t_{air} - T_0) / 10} \quad (44)$$

Where R_{d0} is the respiration rate at the reference temperature T_0 and Q_{10} the temperature coefficient, a factor by which respiration rate changes.

$$Q_{10} = 3.22 - 0.046t_{air} \quad (45)$$

In the model, a variable Q_{10} was used to give respect to decreased respiration rates at low and high temperatures.

For calculation the assimilation rate, intercellular CO₂ concentration c_i was used. It is assumed that CO₂ diffusion into the leave equals the assimilation rate (A_{total}). The process of net CO₂ flux can then also be described as a diffusion process:

$$A_{total} = g_{lc}(c_a - c_i) \quad (46)$$

where c_a is the ambient CO₂ concentration. Following this, Eq. 39 is then rearranged to c_i and substituted into the photosynthesis model, to get a quadratic equation for c_i (Bonan 2019a):

$$g_{lc}c_i^2 + [a - R_d + (a - R_d)/g_{lc}]c_i - [a\Gamma + (c_a g_{lc} + R_d)b] = 0 \quad (47)$$

with $a=v_{c,max}$ and $b=K_C(I+O_2/K_O)$ for A_C -limited assimilation and $a=J/4$ and $b=2\Gamma$ for A_L -limited assimilation. The smaller root is then c_i .

J , describes the electron transport rate, written as:

$$J = \frac{J_{max} s_{rad} c_{rad}}{2.1 J_{max} + s_{rad} c_{rad}} \quad (48)$$

where $J_{max}=1.67v_{c,max}$ is the maximum electron transport rate and c_{rad} is a unit conversion factor for s_{rad} the shortwave downwelling radiation.

The physiological parameters J_{max} , $v_{c,max}$, K_O , K_C and Γ , depending on enzymatic responses. enzyme activity is restricted at low temperatures. The parameter restriction at low temperatures is described by an Arrhenius function (Bernacchi et al. 2001; Bonan 2019a):

$$f(t_{air}) = \exp\left[\frac{\Delta H_a}{298.15\Re}\left(1 - \frac{298.15}{t_{air}}\right)\right] \quad (49)$$

where ΔH_a is the parameter specific activation energy and \Re is the universal gas constant. In the model, no leaf temperature was considered, thereby air temperature (t_{air}) was used. Eq. 42 equals 0, if $t_{air}=25^\circ\text{C}$, here converted to Kelvin. Actual parameter values at a specific temperature are then obtained by multiplying Eq. 43 with the parameter value at 25°C .

Parameters $v_{c,max}$ and J_{max} are also restricted at temperatures above 25°C , written as (Bonan 2019a):

$$f_H(t_{air}) = \frac{1 + \exp\left(\frac{298.15\Delta S - \Delta H_d}{298.15\Re}\right)}{1 + \exp\left(\frac{\Delta S t_{air} - \Delta H_d}{\Re t_{air}}\right)} \quad (50)$$

Where ΔH_d is the energy of deactivation and ΔS an entropy term for v_{cmax25} and J_{max25} , respectively (Farquhar et al. 1980). Subsequently, actual parameter values at a specific temperature are obtained by multiplying the parameter values at 25°C with Eq. 43, and for $v_{c,max}$ and J_{max} in addition with Eq. 44. Values for v_{cmax25} , J_{max25} , K_{O25} , K_{C25} , Γ_{25} are listed in table 1.

11.1.3 Carbon balance

A simplified biomass accumulation approach was used to determine the effects of different root systems on plant success. For that, gross primary production GPP was defined as (Bonan 2019d):

$$GPP = A_{total} m_{carbon} \quad (51)$$

where m_{carbon} is the molar mass of carbon.

NPP was defined as the sum of GPP and a mortality rate M_{total} , including turnover rates for leaves and fine roots (TO_{leaf} , TO_{root}), background mortality M_b , and drought induced mortality M_ψ (He et al. 2012):

$$NPP = GPP - M_{total} \quad (52)$$

with

$$M_{total} = (BM_{total} M_b + BM_{total} M_\psi + TO_{leaf} + TO_{root}) \quad (53)$$

Turnover rates are defined as $1 \text{ yr}^{-1} \text{ g}^{-1}$ with leaf and fine root biomass of 400 g each. M_b is $0.01 \text{ yr}^{-1} \text{ g}^{-1}$ and M_ψ is $0.5 \text{ yr}^{-1} \text{ g}^{-1}$ multiplied with PLC to simulate repair costs for cavitation.

BM_{total} for time step $t+1$ was then:

$$BM_{total,t+1} = BM_{total,t} + NPP * dt \quad (54)$$

with $BM_{total}=10 \text{ kg}$ at the start of the simulations.

11.2 Sensitivity analysis

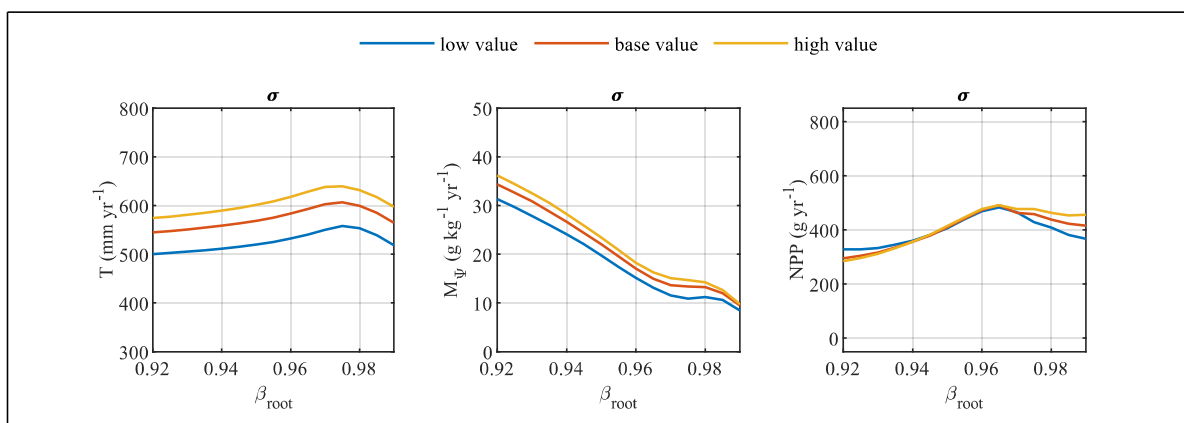


Figure 13 Model output of the parameter σ of the sensitivity analysis; Low, base, and high values are shown in table 9.

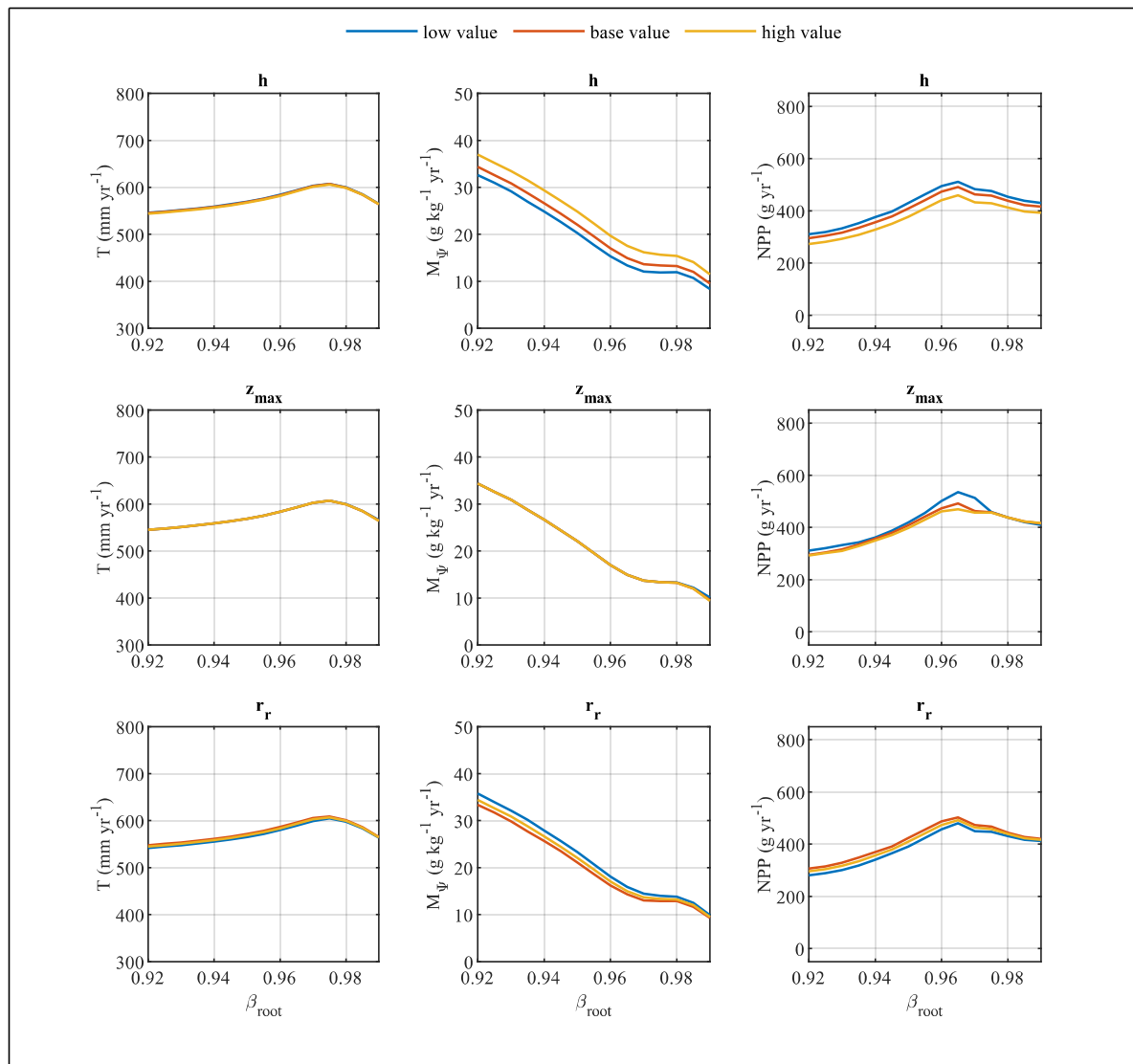


Figure 14 Model output of the parameters h , z_{\max} and r_r of the sensitivity analysis; Low, base, and high values are shown in table 9.

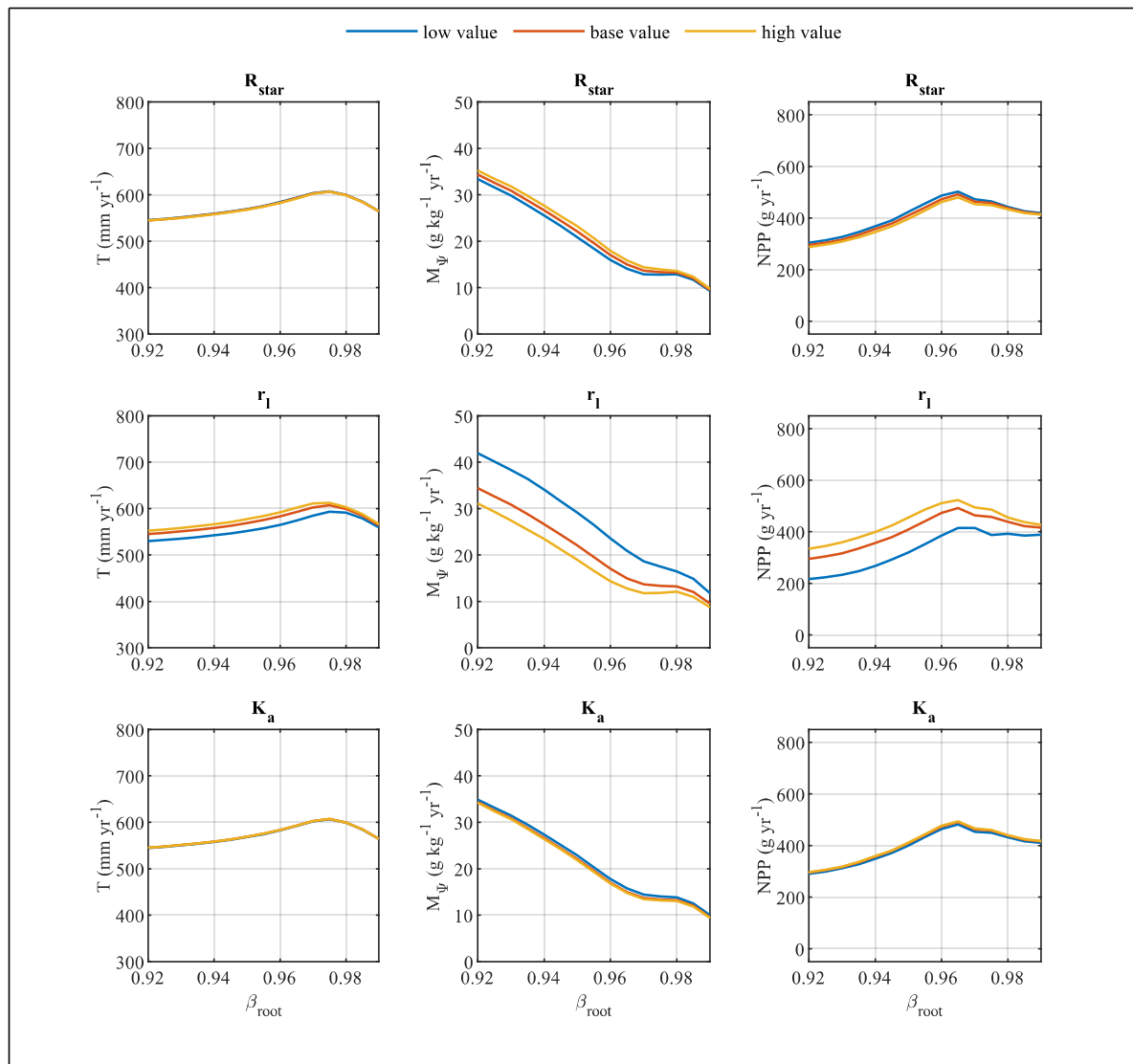


Figure 15 Model output of the parameters R_{r^*} , r_l and K_a of the sensitivity analysis; Low, base, and high values are shown in table 9.

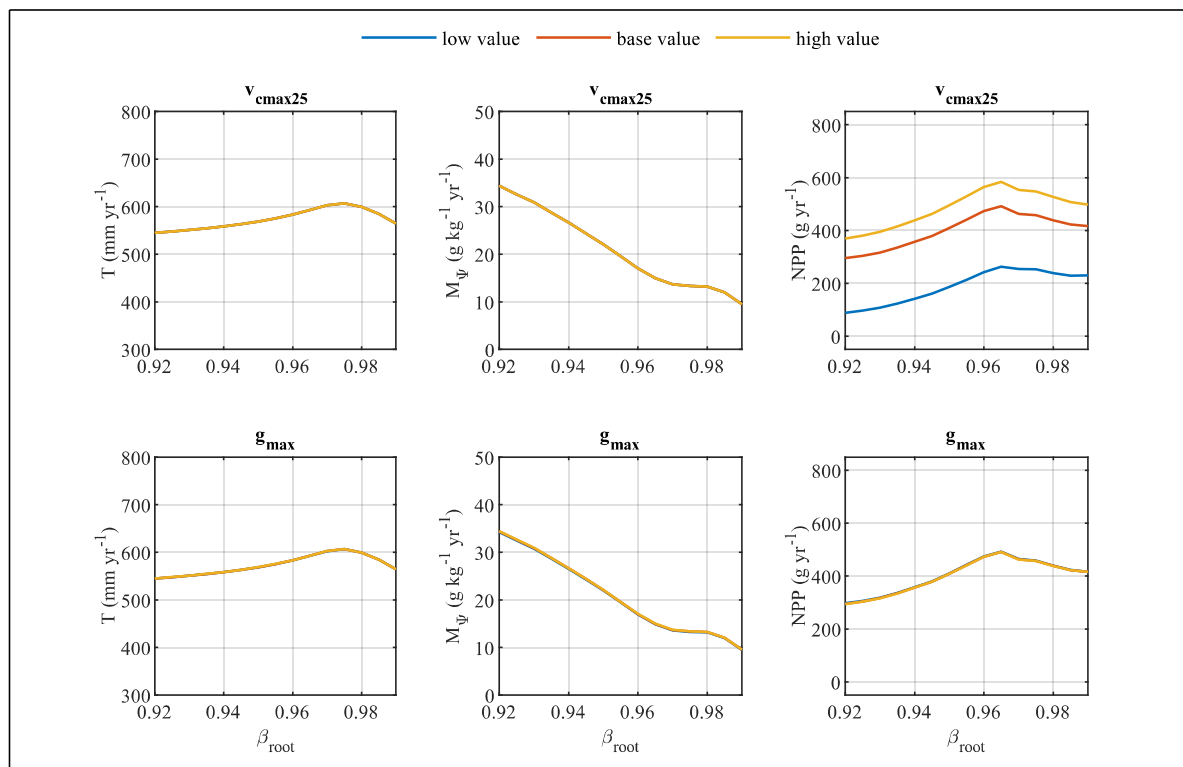


Figure 16 Model output of the parameters v_{cmax25} and g_{max} of the sensitivity analysis; Low, base, and high values are shown in table 9.

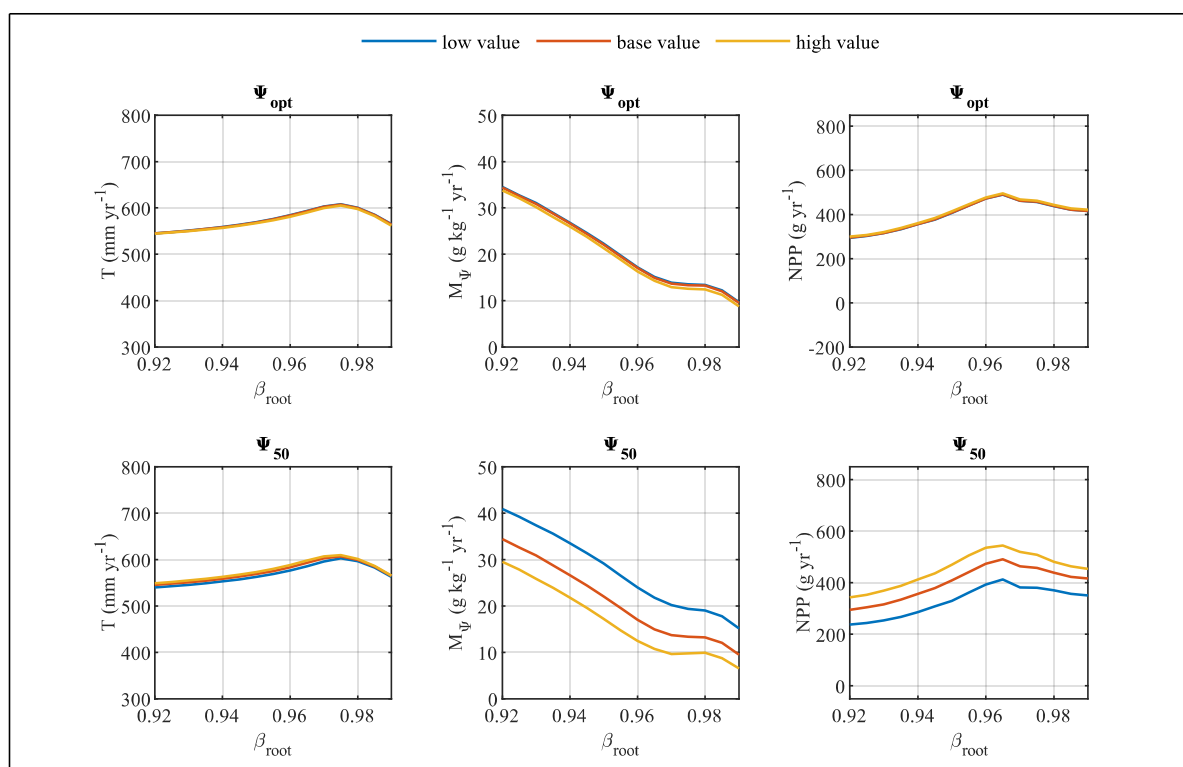


Figure 17 Model output of the parameters Ψ_{opt} and Ψ_{50} of the sensitivity analysis; Low, base, and high values are shown in table 9.

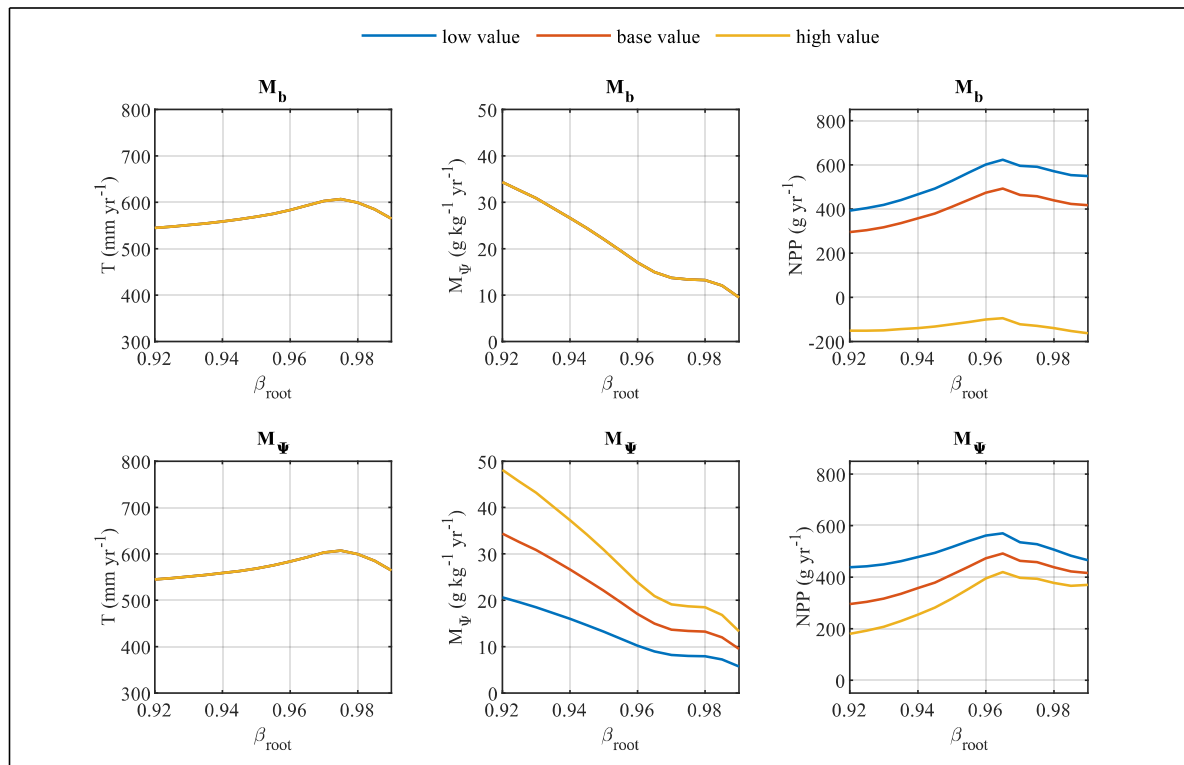


Figure 18 Model output of the parameters M_b and M_ψ of the sensitivity analysis; Low, base, and high values are shown in table 9.